American Mineralogist, Volume 72, pages 1097–1121, 1987

Alteration of amphibolitic wallrocks around the Tanco rare-element pegmatite, Bernic Lake, Manitoba

George B. Morgan VI, David London
School of Geology and Geophysics, University of Oklahoma, Norman, Oklahoma 73019, U.S.A.

Abstract

Amphibolitic wallrocks around the Tanco rare-element pegmatite record three episodes of metasomatic alteration by pegmatite-derived fluids. The apparent sequence of alteration was (1) B (± Li) metasomatism (tourmalinization), (2) K-Rb-Cs-F (± Li) metasomatism (formation of metasomatic biotite), and (3) propylitic alteration (Hbl + Pl → Ep + Chl + Ttn + Cal + clay) with concomitant influx of Li and CO_2. Holmquistite is present in all three metasomatic assemblages and served as the primary sink for Li. Wallrock metasomatism was preceded by an episode of textural recrystallization at lower-amphibolite-facies conditions. Recrystallization may have been caused by heat loss from the pegmatite, but is more probably an artifact of pre-emplacement metamorphism. All metasomatic alteration that is clearly pegmatite-related took place at greenschist-facies conditions ($T \leq 500$–550 °C, $P \leq 300$ MPa). The B-rich fluid that caused tourmalinization of wallrocks was generated by the crystallization of albitites within the pegmatite. Fluids responsible for K-Rb-Cs-F (± Li) metasomatism of wall rocks (at $T = 450$–460 °C) were generated by (1) liberation of acidic, F-rich fluid by the late crystallization of albitites and (2) consequent sericitization of pegmatitic microcline and pollucite. Log (f_{HF}/f_{H_2O}) of fluids in equilibrium with exomorphic biotite at the pegmatite contact was −4.9 at $T = 400$–500 °C and approached negative infinity within 4 m from the pegmatite. Internal pegmatite fluids equilibrated with primary amblygonite-montebrasite ($X_{amb} = 0.40$) at 600 °C record log (f_{HF}/f_{H_2O}) = −4.8. Propylitic alteration, the most pervasive type of alteration around Tanco, occurred throughout the entire episode of wallrock metasomatism, but became dominant when solute-depleted pegmatite fluids cooled to $T \leq 420$ °C.

Through the documentation of the modal abundance and crystal chemistry of metasomatic and retrograde phases, the total masses of B, F, and alkalis lost from the pegmatite have been estimated. The calculated masses represent significant proportions of these components in the original pegmatite magma.

Introduction

The development of genetic models relating pegmatite evolution to wallrock exomorphism has been hindered by the complexity of pegmatite geology (e.g., Jahns, 1982; Černý, 1982a, 1982b), by poor understanding of internal pegmatite evolution, and by incomplete documentation of both internal pegmatite zonation and wallrock alteration. The Tanco pegmatite deposit near Bernic Lake, Manitoba, provides a unique opportunity to relate wallrock alteration to internal evolution and to assess the alteration aureoles in three dimensions. Tanco is unusually well exposed by extensive mining, and its internal zonation and mineralogy are well documented by the mine geologists and by Dr. Petr Černý and colleagues (see references in Černý, 1982a; Černý et al., 1985). The cooling history and internal evolution of Tanco have been ascertained through fluid-inclusion and phase-equilibrium studies (London, 1982, 1984b, 1985, 1986a: London and Burt, 1982a). The pegmatite has been penetrated both top and bottom by over 400 cored drill holes, providing unparalleled control of pegmatite–host rock contacts. Finally, the pegmatite is hosted by a single hornblende-plagioclase amphibolite, so that the interpretations of pegmatite fluid chemistry from wallrock alteration are not complicated by large variations in the bulk compositions of host rocks.

On the basis of the above data and knowledge, this study provides the most complete record to date of wallrock alteration around a large, rare-element pegmatite. Moreover, this work breaks new ground in systematically relating wallrock alteration to internal pegmatite evolution in terms of P-T conditions, melt-vapor evolution, and the mass of pegmatite components lost from magma to wallrocks. The study focuses on the behavior of alkalis, F, and especially B, for which reconnaissance tourmalinization experiments are cited. The results are pertinent to models of pegmatite evolution, to pegmatite exploration, and to the general behavior of volatile and other mobile components in highly differentiated, hydrous silicic magmas.

0003–004X/87/1112–1097$02.00

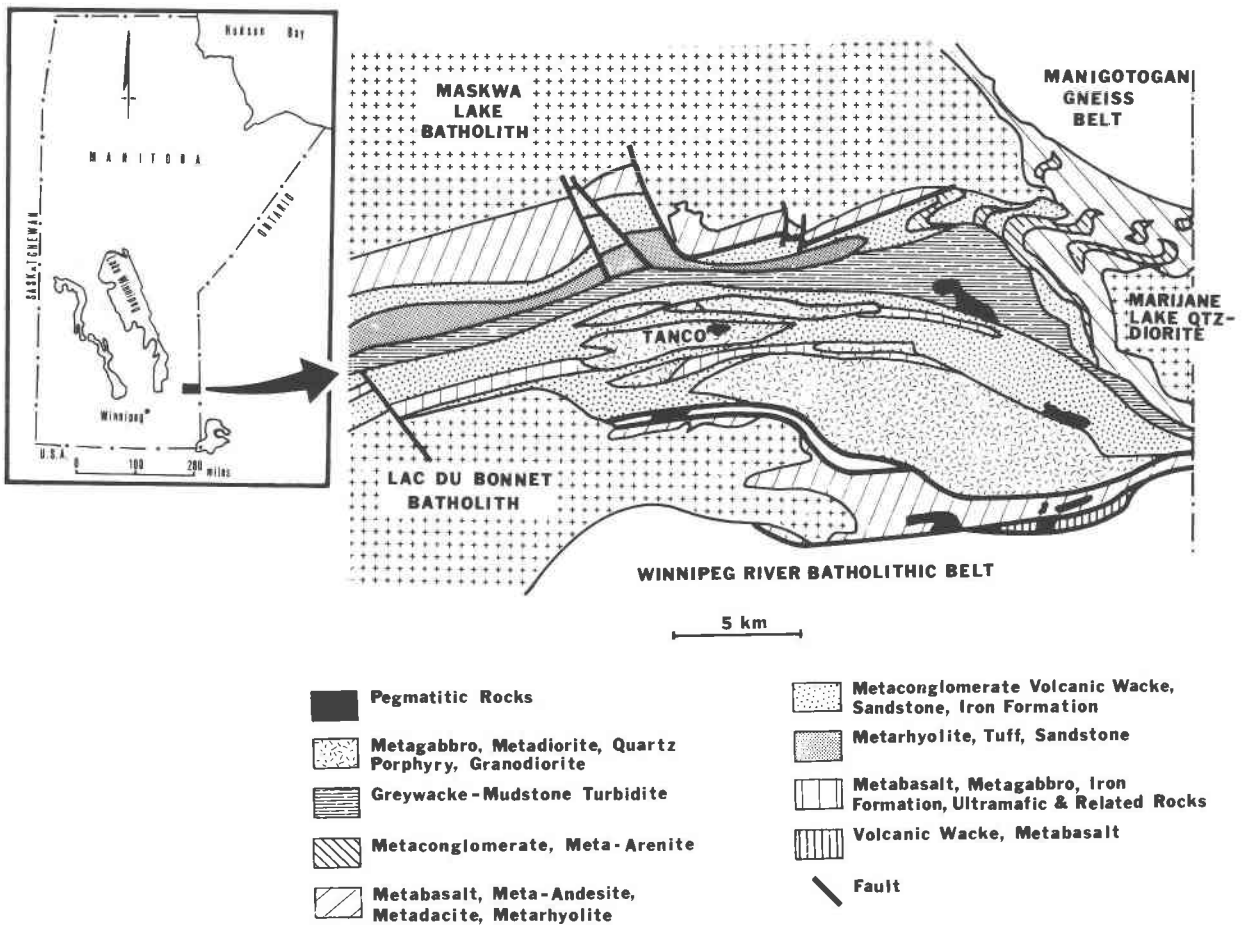

Fig. 1. Location of, and regional geology around, the Tanco pegmatite, southeastern Manitoba (after Černý, 1982a).

Previous work

Though the internal zonation and petrology of the Tanco pegmatite are well documented (Hutchinson, 1959; Wright, 1963; Crouse and Černý, 1972; Černý, 1982a), wallrock alteration around the deposit has been virtually unstudied. Wright (1963) described the characteristics of wallrock alteration from just three cores in the hanging-wall amphibolite above the north-central portion of the body. Even with this limited sample, Wright (1963) observed that the nature and extent of wallrock alteration varied with location, as would be expected from studies of other deposits (cf. Ovchinnikov, 1976; Shearer et al., 1984, 1986). Trueman (1978) noted small, but distinct, Li and Rb whole-rock anomalies in the host rocks above the Tanco pegmatite at distances beyond the obvious metasomatic aureoles.

Location and general geology

The Tanco deposit is located in southeastern Manitoba, approximately 180 km east-northeast of Winnipeg (Fig. 1). It has been a major producer of tantalum for nearly two decades, contains large reserves of rubidium, cesium, gallium, and beryllium, and is currently in production for ceramic-grade spodumene (P. J. Vanstone, Tantalum Mining Corp. of Canada, Ltd., pers. comm., 1986). Tanco is among the most highly fractionated silicic bodies yet discovered (Černý et al., 1985), and its maximum dimensions of approximately 1.4 km (east to west) by 0.82 km (north to south) by 100 m thick make it a giant among complex, rare-element pegmatites. The pegmatite is roughly elliptical in plan view, and forms a bilobate, shallowly north-dipping, and doubly plunging (east and west) body (Černý, 1982a). Even simplified cross sections (Figs. 3 and 4) reveal that the internal zonation of the Tanco pegmatite is far more complex than the simple layered or concentric models of Jahns and Burnham (1969) or Jahns (1982; cf. Norton, 1983).

The nomenclature and descriptions of the internal zones of the pegmatite have varied among different researchers and mine geologists over time. In this study, we have used the terminology as it currently exists on Tanco core logs and geologic sections. In terms of the present mine geologists, the deposit is composed of multiple occurrences of eight internal units: albitic aplites (albitites); central intermediate zones; lepidolite units; mixed zones;

TABLE 1. Distribution of minerals in the internal units of the Tanco pegmatite, Manitoba

	Albitites	Central intermediate zones	Lepidolite units	Mixed zones	Pollucite bodies	Quartz bodies	Spodumene-quartz zones	Wall zones
Albite	P(60)†	M(5)	v(10)	M(15)	a(5)	r(2)	v(4)	P(60)†
Quartz	M(30)	M(15)	a(10)*	M(32)	v(10)*	P(92)†	M(30)†	M(35)
Microcline-perthite	—	P(55)†	v(2)	M(25)	r(2)	r(2)	a(4)*	M(15)
Primary muscovite	v(3)*	a(5)	—	v(4)	—	r(0)	—	a(5)
Secondary (hydrothermal) muscovite	—	a(15)	P(75)†	a(7)*	a(2)	—	a(1)	—
Lepidolite	—	a(0)	a(5)†	r(0)	r(0)	—	—	—
Spodumene	a(0)	a(0)	—	M(9)	a(0)*	r(1)	P(50)†	—
Petalite	—	—	—	r(0)	r(0)	—	r(0)	—
Eucryptite	—	—	—	—	—	—	r(0)	—
Amblygonite-montebrasite	—	—	—	v(2)	r(0)	r(2)	v(10)†	—
Triphylite-lithiophilite	—	a	—	a*	—	r	a*	a
Beryl	a(0)†	v(3)	a(0)†	a(1)	—	—	—	a(1)
Pollucite	—	r(0)	—	—	P(80)†	r	a(0)*	—
Tantalum oxides	a(1)†	r(0)	a(<1)†	r(<1)	—	—	r(0)	a(1)
Cassiterite	a	r	a	—	—	—	—	—
Zircon-hafnon	r	—	r	—	—	—	—	—
Ilmenite	r	—	—	—	—	—	—	—
Tourmaline	a(1)*	—	—	—	—	—	—	v(1)*
Apatite	a	a	a	a	r	—	—	a
Garnet	a(1)	—	—	—	—	—	—	a(0)

Note: Mineral proportions are indicated by P—principal or most important phase (usually >50 vol%); M—major phase (>15 vol%); v—variable abundance from major to accessory phase; a—accessory phase (<5 vol%); r—rare phase. Values in parentheses are estimated modal proportions used in derivation of the pegmatite composition for mass-balance considerations. The mineral abundances of all units are modified after Černý (1982a) and Crouse and Černý (1972), with suggestions by P. J. Vanstone (Tantalum Mining Corp., pers. comm., 1986).

* A subordinate or accessory phase that is characteristic of the zone indicated.

† Mineral that may occur in economic concentrations in the zones indicated.

pollucite bodies; quartz bodies; spodumene-quartz intergrowth zones; and wall zones. The typical mineral assemblages of these units are listed in Table 1. The wall zone includes a thin "rind" of border zone; border and wall zones are not distinguished in this study (cf. Černý, 1982a; Crouse and Černý, 1972). The central intermediate zone consists mostly of microcline ± quartz, but locally contains volumetrically minor albitite (Černý, 1982a). The mixed zone roughly correlates with the lower intermediate zone of Černý (1982a) and Crouse and Černý (1972) and contains variable proportions of albitite, spodumene-quartz zone, and central intermediate zone. The spodumene-quartz zone is correlative with the spodumene-rich upper intermediate zone of Černý (1982a) and Crouse and Černý (1972). All of the internal units except the lepidolite and albitite units have been considered to be of primary (magmatic) origin (Hutchinson, 1959; Wright, 1963; Černý, 1982a). The lepidolite units have been interpreted in the same studies as replacements of the central intermediate zone. These early studies also regarded the albitites as replacement bodies, but more recent interpretations based on petrologic fabrics and fluid-inclusion analyses have demonstrated a primary origin for these units as well (Thomas and Spooner, 1984, 1985; P. J. Vanstone, pers. comm., 1985; Petr Černý, pers. comm., 1985; London, 1986a). In addition to the lepidolite units, microcline in the central intermediate zone, spodumene-quartz zone, and mixed zone has been extensively altered to muscovite (Mus ≤ 85 vol% in the central intermediate zone: P. J. Vanstone, pers. comm., 1986).

Within the limits of exploration, the Tanco pegmatite is completely enclosed by weakly foliated to well-foliated plagioclase amphibolites of the Archean Bird River greenstone belt (Fig. 1). The foliation strikes E-W and dips 70°–85°S; hence, the pegmatite cuts the foliation and layering of the amphibolite at an angle of nearly 90° (Wright, 1963). The peak of regional metamorphism, which predated emplacement of the pegmatite (Černý, 1982a), reached lower-amphibolite facies in the rocks immediately surrounding the pegmatite (Černý, 1982a; cf. Moody et al., 1983). Emplacement of the pegmatite appears to have been controlled by subhorizontal joints and fractures in the host amphibolite (Černý, 1982a; Brisbin and Trueman, 1982).

SAMPLING AND ANALYTICAL PROCEDURES

Twenty-three drill cores were selected from the Tanco core library for this study (Fig. 2), yielding 22 transects away from the hanging-wall contact and 20 transects away from the footwall. Where available, the first 1 to 3-m of amphibolite core adjacent to the pegmatite were sampled. In all holes, the first 1- and 0.3-m intervals of core at approximately 2, 3.5, 5.5, 7, and sometimes 9 m away from the pegmatite were sampled. This allowed sampling of both altered and unaltered amphibolite in most cores, as alteration is largely confined to within 6 m of the pegmatite contact. Care was taken to avoid core samples that may have been affected by other pegmatite dikes that are subparallel to the main Tanco body (and lie mostly below it). Several 0.3- to 1.0-m intervals of core were taken up to 43 m above the north, east, and west margins of the pegmatite, to provide background control for comparison with both altered and apparently unaltered amphibolite closer to the pegmatite. An important point for this study is that individual vertical drill holes

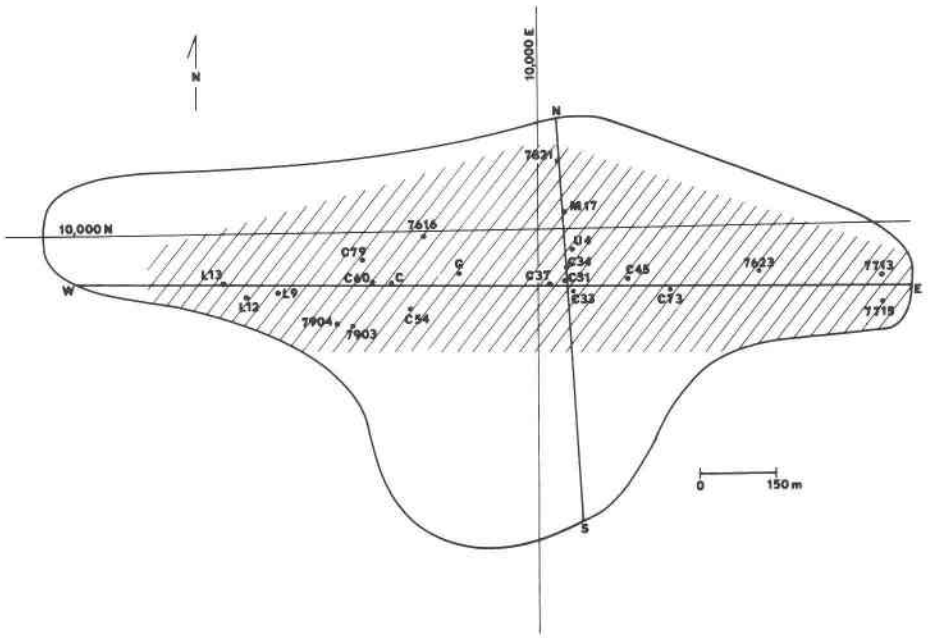

Fig. 2. Approximate plan view of the Tanco pegmatite, showing the locations of drill cores selected for sampling. Lines W-E and N-S show the approximate traces of cross sections represented in Figs. 3 and 4. Cross-hatched area shows portion of the pegmatite for which wallrock alteration is determined and mass-balance calculations are addressed.

penetrate essentially one single metamorphic layer of uniform composition.

Thin sections (175) were primarily studied in transmitted light. Split core samples (especially continuous cores) were also studied in reflected light to qualitatively examine the samples in areas between thin section locations. Qualitative elemental analyses of wallrock phases and pertinent experimental products (discussed below) were obtained on an ETEC Autoscan SEM with PGT System III energy-dispersive spectrometer (EDS) at the University of Oklahoma. Quantitative electron-microprobe analyses (EMPA) were obtained on a JEOL 733 Superprobe at Southern Methodist University, Dallas, Texas. The electron microprobe was operated at an accelerating voltage of 15 kV, using a beam current of 20 nA (except for micas, where 10 nA was used to minimize volatilization of alkalis), and a spot size of 10 μm; data reduction employed the Bence-Albee (Bence and Albee, 1968) correction program. Individual microprobe analyses of the alteration minerals (264 individual microprobe analyses; multiple points per analysis) are given in Table 2,[1] and summed compositional averages are presented in Tables 3–6. Li and total Fe analyses of a few biotite and tourmaline samples were performed by inductively coupled plasma, and Fe^{2+} analyses of the same phases were determined by titration at Skyline Labs, Denver.

Petrology of the unaltered host amphibolite

Fifty samples showing no microscopic evidence of mineral alteration yield a modal composition of 54% hornblende [ferro-hornblende in the terminology of Leake (1968) and Hawthorne (1981); Table 3], 37% plagioclase (An_{27-70}; avg. = An_{38}; Table 3), 4% ilmenite, and 1% apatite. The remaining 4% is composed of quartz, biotite, epidote group minerals, titanite, garnet, and chlorite. The mineral mode of the host amphibolite varies only slightly around the pegmatite. Compositional variability is greater between layers (i.e., different drill cores) than within individual layers (i.e., a single drill core).

The texture of the amphibolite varies from medium-grained ($\leq$3.0 mm) and weakly-foliated to very fine grained ($\leq$0.2 mm), strongly foliated, and gneissically banded. Medium-grained (0.5–1.0 mm), weakly foliated fabrics predominate around most of the pegmatite, with the very fine-grained (0.05–0.1 mm) gneissic variety abundant around the eastern end of the deposit. Schistosity in the medium- and fine-grained amphibolite is characterized by lineation of subhedral blue-green hornblende prisms and plagioclase laths, about one-third of which show albite twinning. Schistosity in the very fine grained amphibolite is manifested by alignment of subhedral to anhedral hornblende prisms that are interlayered with untwinned, saccharoidal plagioclase.

Petrology, distribution, and geochemistry of alteration

Petrographic studies show that there are four types of alteration of host rocks around the Tanco pegmatite; these apparently occurred in the sequence (1) textural recrystallization, (2) B ($\pm$ Li) metasomatism, (3) K-Rb-Cs-F ($\pm$ Li) metasomatism, and (4) propylitic alteration with concomitant influx of Li and CO_2. Detailed petrologic descriptions of these alteration types are given below. Re-

[1] To obtain a copy of Table 2, order Document AM-87-359 from the Business Office, Mineralogical Society of America, 1625 I Street, N.W., Suite 414, Washington, D.C. 20006, U.S.A. Please remit $5.00 in advance for the microfiche.

TABLE 3. Electron-microprobe analyses of hornblende and plagioclase from proximal and distal amphibolites

	1 Average distal hornblende	2 Average proximal hornblende	3 Hornblende C73-FWD	4 Hornblende C73-FWP		5 Average distal plagioclase	6 Average proximal plagioclase	7 Plagioclase C73-FWD	8 Plagioclase C73-FWP
	Oxides (wt%)					Oxides (wt%)			
SiO_2	44.68(2.10)	44.21(2.40)	43.43(0.62)	42.79(0.20)	SiO_2	57.48(3.06)	55.98(2.59)	59.84(1.06)	56.11(0.80)
Al_2O_3	10.58(1.47)	11.73(1.72)	12.70(0.48)	13.60(0.18)	Al_2O_3	26.84(2.09)	28.21(1.96)	25.21(0.86)	27.48(0.85)
MgO	8.31(2.40)	7.89(2.33)	6.77(0.11)	6.44(0.16)	CaO	8.39(2.24)	9.60(2.71)	6.30(1.12)	9.24(0.57)
FeO*	20.06(3.04)	19.95(2.76)	21.65(0.03)	21.17(0.14)	SrO	0.11(0.04)	0.09(0.05)	0.11(0.02)	0.12(0.03)
TiO_2	0.71(0.61)	0.57(0.09)	0.48(0.05)	0.57(0.04)	BaO	0.02(0.03)	0.04(0.05)	0.00(0.01)	0.03(0.04)
MnO	0.30(0.08)	0.30(0.05)	0.24(0.01)	0.28(0.02)					
CaO	10.81(0.50)	10.88(0.67)	10.25(0.32)	10.86(0.26)	Na_2O	6.67(1.40)	5.65(1.36)	7.79(0.28)	6.16(0.36)
Na_2O	1.17(1.24)	1.24(0.23)	1.35(0.04)	1.37(0.05)	K_2O	0.12(0.17)	0.11(0.16)	0.37(0.27)	0.07(0.02)
K_2O	0.33(0.15)	0.37(0.12)	0.33(0.03)	0.39(0.03)	Rb_2O	0.02(0.02)	0.04(0.07)	0.00(0.00)	0.01(0.02)
Rb_2O	0.06(0.09)	0.03(0.02)	0.06(0.02)	0.00(0.00)	Cs_2O	0.02(0.03)	0.02(0.03)	0.00(0.02)	0.02(0.02)
Cs_2O	0.02(0.03)	0.02(0.03)	0.00(0.00)	0.00(0.00)					
F	0.07(0.06)	0.22(0.14)	0.06(0.04)	0.10(0.02)	FeO*	0.29(0.31)	0.20(0.16)	0.23(0.10)	0.13(0.05)
Total	97.10	97.41	97.32	97.57	Total	99.96	99.84	99.85	99.36
	Cations per 23 oxygens					Cations per 8 oxygens			
Si	6.78(0.19)	6.71(0.22)	6.61(0.02)	6.64(0.03)	Si	2.57(0.16)	2.49(0.11)	2.68(0.05)	2.52(0.03)
^{IV}Al	1.22(0.17)	1.29(0.24)	1.39(0.03)	1.36(0.03)	^{IV}Al	1.42(0.12)	1.51(0.11)	1.32(0.06)	1.48(0.03)
Tet. sum	8.00	8.00	8.00	8.00	Fe	0.01(0.01)	0.01(0.01)	0.01(0.01)	0.00(0.01)
					Tet. sum	4.00	4.01	4.01	4.00
^{VI}Al	0.66(0.12)	0.82(0.15)	0.89(0.02)	1.11(0.02)	Ca	0.40(0.11)	0.48(0.10)	0.34(0.05)	0.45(0.02)
Mg	1.70(0.45)	1.58(0.44)	1.30(0.02)	1.10(0.02)	Sr	0.00(0.00)	0.00(0.00)	0.00(0.00)	0.00(0.00)
Fe	2.56(0.44)	2.54(0.40)	2.76(0.01)	2.72(0.02)	Ba	0.00(0.00)	0.00(0.00)	0.00(0.00)	0.00(0.00)
Ti	0.08(0.07)	0.06(0.02)	0.05(0.01)	0.07(0.01)					
M1 + M2 + M3	5.00	5.00	5.00	5.00	Na	0.58(0.12)	0.49(0.11)	0.67(0.04)	0.54(0.03)
					K	0.00(0.01)	0.01(0.02)	0.02(0.01)	0.00(0.01)
Ca	1.76(0.09)	1.77(0.14)	1.67(0.02)	1.80(0.03)	Rb	0.00(0.00)	0.00(0.00)	0.00(0.00)	0.00(0.00)
Mn	0.04(0.01)	0.04(0.01)	0.03(0.00)	0.03(0.01)	Cs	0.00(0.00)	0.00(0.00)	0.00(0.00)	0.00(0.00)
Mg	0.17(0.07)	0.20(0.06)	0.24(0.02)	0.43(0.02)					
M4 sum	1.97	1.99	1.94	2.16	Total	4.98	4.99	5.04	4.98
					An†	41.2(11.8)	49.7(11.4)	33.7(5.3)	45.4(2.0)
Na	0.34(0.07)	0.36(0.07)	0.40(0.01)	0.41(0.01)	Al/(Al + Si)	0.22	0.24	0.26	0.27
K	0.06(0.03)	0.07(0.02)	0.06(0.01)	0.07(0.01)					
A sum	0.40	0.43	0.46	0.48					
Total	15.37	15.44	15.49	15.78					
Mg/(Mg + Fe)	0.42	0.41	0.36	0.36					
Al/(Al + Si)	0.22	0.24	0.26	0.27					

Note: Values in parentheses represent one standard deviation from the mean. The columns show averaged analyses and analyses from a single representative core, as follows: (1) average of 109 analyses of hornblende in distal amphibolite from 11 different cores, (2) average of 83 analyses of hornblende in proximal amphibolite from 10 different cores, (3) average of 9 analyses from the distal portion of footwall core C-73, (4) average of 14 analyses from the proximal portion of footwall core C-73, (5) average of 90 analyses of plagioclase in distal amphibolite from 10 different cores, (6) average of 93 analyses of plagioclase in proximal amphibolite from 9 different cores, (7) average of 10 analyses from the distal portion of footwall core C-73, (8) average of 17 analyses from the proximal portion of footwall core C-73.

* Total Fe is reported as FeO.

† Anorthite content.

crystallized amphibolites are veined and replaced by all three metasomatic assemblages, so that textural recrystallization was unquestionably earlier than the metasomatic-alteration events. In the recrystallized zone, subsequent fluid flow from the pegmatite was partly channeled by a system of fractures that intersect the pegmatite surface at acute angles (from essentially 0° to 45°); intergranular infiltration was prevalent near the pegmatite contacts. Beyond the recrystallized zone, fluid flow and attendant metasomatism occurred along this same system of fractures and along steeply dipping foliation surfaces.

The temporal sequence of B and K-Rb-Cs-F metasomatic events is equivocal because crosscutting textural relationships between the two assemblages are difficult to interpret and do not always suggest the same sequence. These two metasomatic events may have been essentially coeval. In the hanging wall of the central ore zone, where a large pollucite body is in direct contact with the amphibolite (holes C34 and C45), tourmaline is clearly embayed and veined by a later assemblage of muscovite ± biotite + apatite + quartz ± hematite, and biotite is present in the interstices between tourmaline grains. At this location, B metasomatism clearly preceded K-Rb-Cs-F metasomatism. Propylitic alteration apparently accompanied both other types of metasomatic alteration as fluids reacted with the wallrocks, cooled, and became solute-depleted with distance from the pegmatite. Both metasomatic tourmaline and biotite are veined and/or replaced by the propylitic assemblage, showing that widespread propylitic alteration was unquestionably the latest type of alteration. It is this late, widespread episode of propylitic alteration that is referred to as the fourth principal type of wallrock alteration.

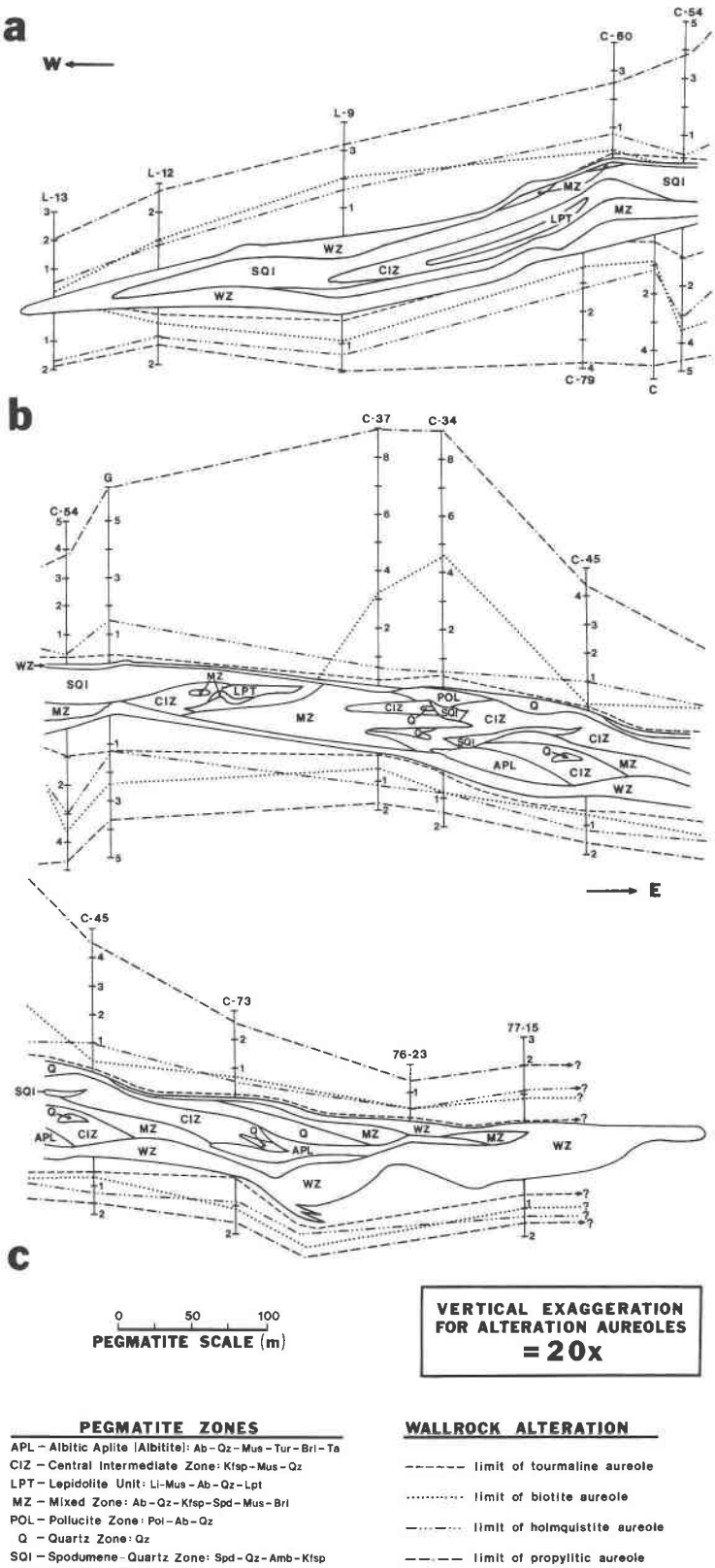

Fig. 3. Vertical cross sections along line W-E in Fig. 2, showing the limits of exomorphic aureoles (wallrock alteration) and their relationship to internal pegmatite zonation: (a) western ore zone, (b) central ore zone, (c) eastern ore zone.

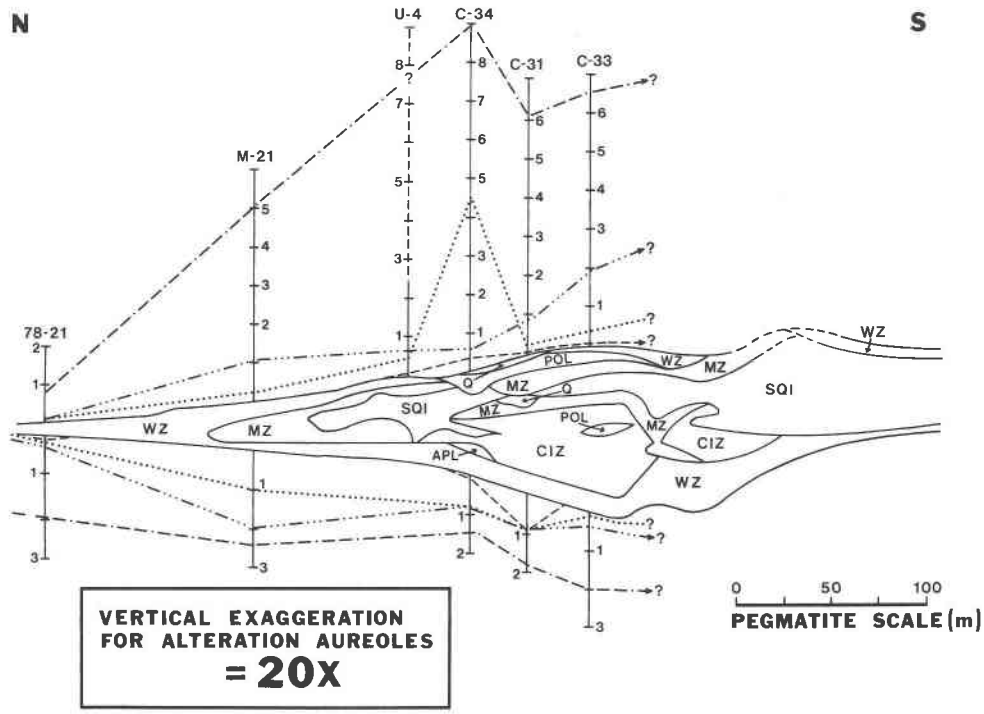

Fig. 4. Vertical cross section along line N-S in Fig. 2, showing the limits of exomorphic aureoles (wallrock alteration) and their relationships to internal pegmatite zonation. All symbols are the same as in Fig. 3.

Figures 3 and 4 show the distributions of alteration aureoles and their relations to internal pegmatite zonation along central cross sections through the width and length of the pegmatite body. The alteration aureole (based on petrology) is extremely narrow in comparison with the thickness of the pegmatite. The distribution of alteration types and the pervasiveness of alteration are exceedingly variable with location around the pegmatite; there are, however, some systematic differences between hanging-wall and footwall alteration (Morgan and London, 1985). Much of the spatial variability of wallrock alteration stems from the fact that alteration assemblages commonly reflect the adjacent internal mineral content of the pegmatite, as discussed in following sections.

Textual recrystallization

Localized along the pegmatite contact is a zone characterized by coarsening of hornblende and plagioclase grains in the amphibolite, with destruction of its characteristic foliation. Within the zone, plagioclase shows albite twinning (in contrast to its typical untwinned, saccharoidal habit), and hornblende commonly contains very fine grained Fe-Ti oxide exsolution lamellae along cleavage surfaces. In addition to these textural changes, a comparison of the modal mineral contents of about 30 samples of the recrystallized, coarser-grained amphibolite with modal abundances in the distal amphibolite demonstrates some minor differences as well. The modal ratio of hornblende/plagioclase is slightly greater in the recrystallized amphibolite. The recrystallized amphibolite also contains a slightly higher abundance of quartz ($\leq$5 vol%) and little or no apatite. These textual and modal differences in the amphibolite along the pegmatite contact present the possibility that recrystallization may have been caused by heat loss from the pegmatite.

Table 3 contrasts averaged EMPA of hornblende and plagioclase, from proximal (i.e., "recrystallized") and distal amphibolites. Both plagioclase (An_{25-70}) and hornblende [atomic ratios: Na/Ca = 0.14–0.30, Mg/(Mg + Fe) = 0.30–0.53, Al/(Al + Si) = 0.19–0.27] show considerable compositional variability in both textural varieties of amphibolite, to the point that no significant compositional differences are immediately obvious between the two. Comparisons of plagioclase and hornblende compositions within a single core (i.e., essentially the same metamorphic layer; Table 3), however, reveal slight but consistent compositional differences between distal (samples C73-FWD) and proximal (samples C73-FWP) amphibolites. In six of eight analyzed amphibolite pairs, plagioclase in recrystallized amphibolite has a higher An content (avg. increase of about 10 mol% An) when compared to that of the distal amphibolite from the same drill hole. Proximal hornblende usually shows small increases in Al_{total}, Mn, Ca, Na, K, F, and Al/Si, slight decreases in Si, Mg, and Mg/(Mg + Fe); Rb and Cs are at or below detection levels in both textural varieties of amphibolite. Relative changes in Fe and Ti contents are variable and usually small (Fe $\leq$ 1.5 wt%; Ti $\leq$ 0.18 wt%). Higher K and F (>0.10 wt%) contents and lower Mg content of proximal hornblende is attributable to re-equilibration

with later pegmatite-derived fluids, based on associated metasomatic mineral assemblages. The compositional trends observed in the proximal amphibolite appear to reflect slightly higher *P-T* conditions that the average distal amphibolite (Moody et al., 1983; Spear, 1977; Leake, 1965; Engel and Engel, 1962). The stability of a calcic ferro-hornblende and an intermediate plagioclase in the presence of ilmenite and quartz, and in the absence of chlorite, epidote, and titanite, suggests that recrystallization must have occurred at least under lower-amphibolite-facies conditions (cf. Moody et al., 1983). The fugacity of oxygen was probably near the NNO buffer (cf. Moody et al., 1983).

Despite minor differences in composition, the overall similarity of proximal (recrystallized) and distal amphibolites suggests that recrystallization occurred in the absence of pegmatite-derived fluids. Because of the evolved composition of the Tanco pegmatite, we would expect that recrystallization in the presence of pegmatite-derived fluids would yield plagioclase with lower An content and hornblende with higher K, Rb, Cs, and F contents as compared to the foliated, distal amphibolite. This interpretation requires either that recrystallization predated emplacement of the pegmatite or that recrystallization occurred before the pegmatite melt evolved a separate, mobile aqueous phase. The lack of significantly lower contents of Ti and Fe in proximal, recrystallized hornblende containing abundant Fe-Ti oxide lamellae (as compared to distal hornblende) suggests that textural recrystallization occurred during regional metamorphism (i.e., at the same grade) and is not a contact-metamorphic effect. The observation of identical oxide exsolution in some distal hornblende also suggests that recrystallization was unrelated to pegmatite heat loss. Although recrystallization is most pronounced near the pegmatite, we suggest that recrystallization preceded pegmatite emplacement (e.g., that the fracture system along which the pegmatite was emplaced served as a channelway for metamorphic fluids that promoted recrystallization prior to pegmatite emplacement).

Boron (± Li) metasomatism

B metasomatism is characterized by the alteration of hornblende + plagioclase ± biotite to tourmaline + quartz ± titanite ± apatite ± calcite ± holmquistite. Tourmaline forms medium- to coarse-grained prisms up to 2.5 mm in diameter and 7 mm in length. Quartz occurs as fine-grained inclusions within tourmaline and as coarse grains interstitial to tourmaline. Small amounts of fine-grained (0.3–0.5 mm) biotite accompany tourmaline in some cores, especially where small pegmatite apophyses intrude the wallrocks. At some locations, particularly in the hanging-wall amphibolite of the eastern central ore zone, tourmaline is intergrown with abundant, coarse-grained calcite (1–2 mm) and titanite (0.5–1.0 mm).

Tourmaline is mostly confined to a narrow aureole 7 to 10 mm wide at the pegmatite-amphibolite contact, but locally penetrates 3 m into the host rock along fractures (veins) or small pegmatite apophyses. The tourmaline aureole almost completely surrounds the pegmatite, but is absent at some locations around the western ore zone and the northern end of the deposit (Figs. 3 and 4). Tourmalinization was most pervasive in the footwall of the eastern ore zone, where voluminous albitites occur in the pegmatite near the lower wall zone. The tourmaline aureole swells eastward beneath the eastern ore zone to hole 7715 (Fig. 3c). It is probable that the tourmaline aureole (as well as the biotite and propylitic aureoles) extends, and possibly expands, beyond the eastern end of the pegmatite, where no core is available. A narrow but pervasive tourmaline aureole also occurs above the pollucite unit in the central ore zone (hole C34; Figs. 3b and 4), and a wide, but less pervasive, aureole lies along the footwall of the western ore zone at hole G (Figs. 3a and 3b).

Metasomatic tourmaline usually displays complex and variable pleochroic zoning. The most common color zonation is that of dark blue or blue-green cores, grading outward through green to brown interior zones and olive-green outer zones and rims. Reversals and variations of this sequence are common, often within a single thin section. Tourmaline from pervasively altered amphibolite above the central ore zone, where a pollucite unit occurs in direct contact with the amphibolite (hole C34), is predominantly uniform yellow-brown, with small blue cores.

The composition of tourmaline is variable (Table 4), falling in the range $Srl_{25-95}Drv_{3-45}Uv_{1-25}Cft_{1-27}$, where Cft represents an end-member tourmaline component (ferro-uvite) with the approximate composition $CaFe^{2+}_3Al_6(BO_3)_3Si_6O_{18}(OH,F)_4$. The $X_{Mg}/X_{(Mg+Fe)}$ ratio in all tourmaline is extremely variable (0.05–1.33) and is usually dissimilar to that of the hornblende it replaces. The Fe_2O_3/FeO weight ratios for a few analyzed tourmalines (from cores C33, C34, and C45) fall in the range 2.3–6.9, a qualitative indication that the metasomatic fluids were oxidizing in nature. Rb and Cs contents in all tourmaline are very low, usually less than about 0.1 wt% Rb and 0.2 wt% Cs. F varies from 0.13–1.39 wt%, with tourmaline from most locations in the low to moderate range (avg. 0.74 wt% F). Two representative blue-cored, green-rimmed tourmalines (from cores C33 and C73) show low Li content (average about 500 ppm). In contrast, the yellow-brown tourmaline from hole C34 contains 5300 ppm Li at the pegmatite contact, decreasing to 1300 ppm 0.3 m away.

The most consistent chemical zonation of tourmaline is that of decreasing Ca content (by about 0.1–0.6 wt%) from core to rim. Zonal variation of X_{Mg}/X_{Fe} within single crystals is slight, commonly decreasing by 0.02–0.30 wt% from core to rim. This trend is reversed in the yellow-brown tourmaline from hole C34. The increasing Mg/Fe ratio from core to rim and the higher Li content of this tourmaline may reflect early crystal growth in a relatively oxidizing environment (incorporation of Fe^{3+} in blue cores: see Foit and Rosenberg, 1979) and subsequent incorporation of Li and Mg as a result of relative depletion in Fe.

The low concentrations of rare alkalis and F in meta-

TABLE 4. Electron-microprobe analyses of tourmaline, averaged with respect to location around the pegmatite

	WOZ	WOZ-Hi F	COZ	COZ-POL	EOZ
			Oxides (wt%)		
SiO_2	34.89(0.04)	35.12(0.30)	34.78(0.48)	35.53(0.42)	34.78(0.99)
Al_2O_3	33.67(0.06)	29.90(1.39)	30.33(1.86)	30.41(1.69)	26.98(0.99)
MgO	0.39(0.02)	4.61(0.86)	4.80(1.94)	4.94(1.03)	4.19(0.73)
FeO*	13.43(0.14)	11.30(0.79)	11.37(1.18)	10.65(1.55)	13.86(1.10)
TiO_2	0.39(0.02)	0.83(0.31)	0.72(0.33)	0.56(0.19)	0.89(0.14)
MnO	0.29(0.03)	0.15(0.05)	0.17(0.15)	0.10(0.02)	0.09(0.02)
CaO	0.05(0.02)	1.10(0.20)	1.23(0.62)	0.75(0.39)	2.09(0.37)
Na_2O	1.82(0.02)	2.14(0.07)	1.70(0.20)	2.32(0.16)	1.37(0.16)
K_2O	0.04(0.01)	0.04(0.01)	0.10(0.17)	0.04(0.01)	0.03(0.01)
Rb_2O	0.03(0.03)	0.00(0.01)	0.01(0.02)	0.07(0.07)	0.01(0.02)
Cs_2O	0.08(0.04)	0.01(0.01)	0.05(0.03)	0.01(0.02)	0.02(0.03)
F	0.51(0.06)	1.05(0.07)	0.40(0.17)	1.19(0.15)	0.74(0.14)
Total	85.59	86.25	85.66	86.57	85.05
			Cations per 29 oxygens		
Si	5.81(0.01)	5.86(0.02	5.79(0.06)	5.87(0.02)	5.90(0.15)
^{IV}Al	0.19(0.01)	0.14(0.01)	0.21(0.03)	0.13(0.01)	0.10(0.04)
Tet. sum	6.00	6.00	6.00	6.00	6.00
Al(18c)**	6.00(0.02)	5.79(0.17)	5.96(0.40)	5.91(0.22)	5.36(0.07)
Al	0.42(0.02)	—	—	—	—
Mg	0.10(0.01)	1.13(0.21)	1.19(0.48)	1.20(0.25)	1.04(0.16)
Fe	1.87(0.02)	1.62(0.05)	1.58(0.18)	1.48(0.24)	1.94(0.16)
Ti	0.05(0.01)	0.10(0.04)	0.09(0.04)	0.07(0.02)	0.11(0.03)
Mn	0.04(0.01)	0.02(0.01)	0.02(0.02)	0.01(0.00)	0.01(0.01)
9b** sum	2.48	2.87	2.88	2.76	3.10
B†	3.00 —	3.00 —	3.00 —	3.00 —	3.00 —
Ca	0.01(0.00)	0.21(0.04)	0.21(0.11)	0.14(0.07)	0.38(0.06)
Na	0.58(0.01)	0.70(0.05)	0.54(0.07)	0.72(0.05)	0.45(0.04)
K	0.01(0.00)	0.01(0.00)	0.01(0.01)	0.00(0.00)	0.00(0.01)
Rb	0.00(0.01)	0.00(0.01)	0.00(0.00)	0.00(0.01)	0.00(0.00)
Cs	0.00(0.00)	0.00(0.01)	0.00(0.00)	0.00(0.00)	0.00(0.00)
3a** sum	0.60	0.92	0.76	0.86	0.83
Total	18.08	18.44	18.39	18.40	18.19
F (pfu)	0.26(0.02)	0.55(0.04)	0.21(0.09)	0.62(0.08)	0.39(0.07)
Na/(Na + Ca)	0.98(0.01)	0.77(0.12)	0.72(0.13)	0.85(0.07)	0.55(0.05)
Mg/(Mg + Fe)	0.05(0.01)	0.41(0.05)	0.41(0.12)	0.44(0.08)	0.35(0.05)
Al/(Al + Si)	0.53(0.02)	0.50(0.05)	0.51(0.14)	0.50(0.06)	0.48(0.03)

Note: All samples were taken within <0.25 m of the pegmatite contact. Sample locations correspond to WOZ—eastern ore zone (9 analyses); WOZ-Hi F—high-F tourmaline from footwall of WOZ at hole C-54 (15 analyses); COZ—central ore zone (21 analyses); COZ-POL—hanging wall of the central ore zone, above the pollucite body (31 analyses); EOZ—eastern ore zone (13 analyses). Values in parentheses represent one standard deviation from the mean.

* Total Fe is reported as FeO.

** Site assignments from Donnay and Buerger (1950): 18c = Z, 9b = Y, 3a = X.

† B is assumed present in stoichiometric proportion.

somatic tourmaline and the paucity of metasomatic biotite and holmquistite in the tourmaline-bearing assemblage are consistent with an origin due to the influx of a comparatively acidic aqueous pegmatitic fluid rich in B and poor in K, Rb, Cs, Li, and F. The temperature at which B metasomatism occurred is uncertain, but three lines of evidence indicate that B metasomatism took place at greenschist-facies metamorphic conditions (≤550 °C). First, tourmalinization was apparently accompanied by propylitic alteration farther from the pegmatite, where solute-depleted fluids reacted with wallrocks without a significant change in bulk-rock composition (i.e., no significant metasomatism other than infiltration of aqueous fluid). Second, hornblende that coexists with metasomatic tourmaline shows no compositional changes indicative of prograde thermal re-equilibration beyond that of textural recrystallization. Finally, the common coexistence of metasomatic biotite and tourmaline and the complex cross-cutting relationships between the two metasomatic assemblages suggest that tourmalinization may have been nearly coeval with K-Rb-Cs-F (± Li) metasomatism, which occurred at approximately 450 °C (see garnet-biotite geothermometry in the discussion of K-Rb-Cs-F metasomatism, below).

K-Rb-Cs-F (± Li) metasomatism

K-Rb-Cs-F (± Li) metasomatism is characterized by the alteration of hornblende ± plagioclase to biotite ± apatite ± holmquistite. Arsenopyrite and monazite (tentative identification) are common accessory minerals. Hornblende was more susceptible to biotitization than plagioclase, but at some locations (e.g., L9-00, C54-101),

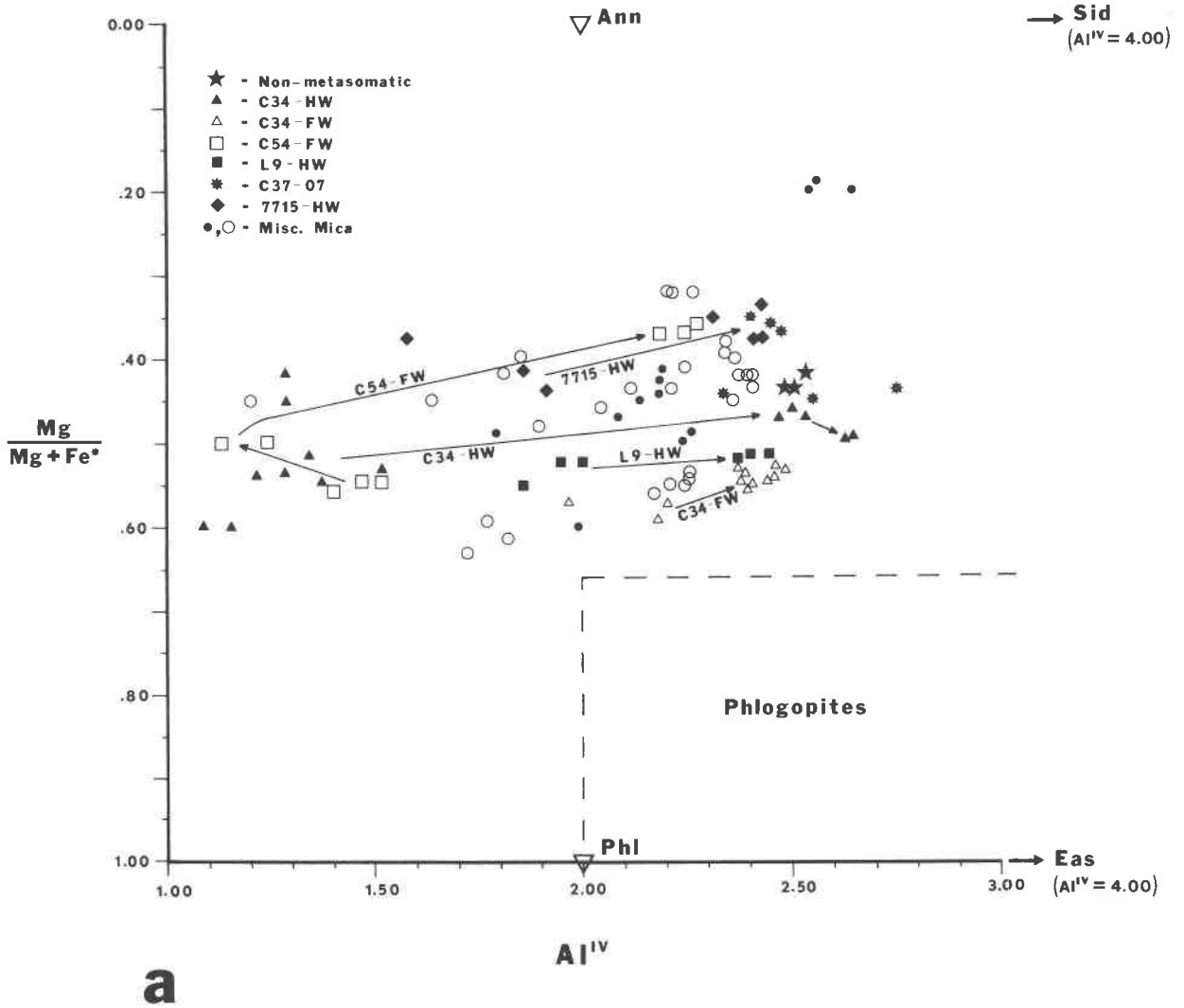

Fig. 5. (a) ^{IV}Al vs. $Mg/(Mg + Fe_{total})$ for exomorphic micas and non-metasomatic micas. (b) $^{IV}Al/Al_{total}$ vs. $(Mg + Mn + Ti + Fe_{total})/6$ for exomorphic micas and non-metasomatic micas. Arrows show the trends of micas from individual drill cores with increasing distance from the pegmatite contact. Ideal compositions of annite, siderophyllite, phlogopite, eastonite, polylithionite, trilithionite, and taeniolite are after Bailey (1984). Ideal composition of zinnwaldite is after Hawthorne and Černý (1982).

even plagioclase was completely converted to biotite. Metasomatic muscovite was found with biotite only in the hanging wall of the central ore zone above the pollucite unit (hole C34). There, earlier pervasive tourmalinization appears to have consumed essentially all of the available Fe and Mg. This resulted in the production of a Rb-rich, Fe-bearing muscovite, which appears to have replaced the Li-rich outer rims of the tourmaline.

K-Rb-Cs-F metasomatism is more pervasive in the footwall than in the hanging-wall amphibolite and locally penetrates 4.5 m into the host rock along fractures or foliation surfaces (Figs. 3 and 4). The aureole of K-Rb-Cs-F metasomatism is discontinuous and commonly less than 1 m thick along the hanging wall, except for particularly wide aureoles over the central ore zone, where a large pollucite body is in direct contact with the host rock, and over the western ore zone. Along the footwall, the biotite aureole is essentially continuous and generally 1 to 3 m thick, except for a rather large and very pervasive aureole (up to 90 vol% biotite) in the western ore zone at drill hole C-54 (Fig. 3). The abundance of metasomatic biotite in the wallrocks usually correlates with regions in the pegmatite where central intermediate and/or mixed zones are located next to the wall zone. This association is also observed above the central ore zone, where the pollucite body is underlain by large volumes of central intermediate and mixed zones. Additionally, the central intermediate and mixed zones usually contain or lie in close proximity to albitites.

Electron-microprobe analyses of exomorphic biotite are averaged with respect to distance from the pegmatite contact in Table 5. The Mg/(Mg + Fe) ratios in all of these

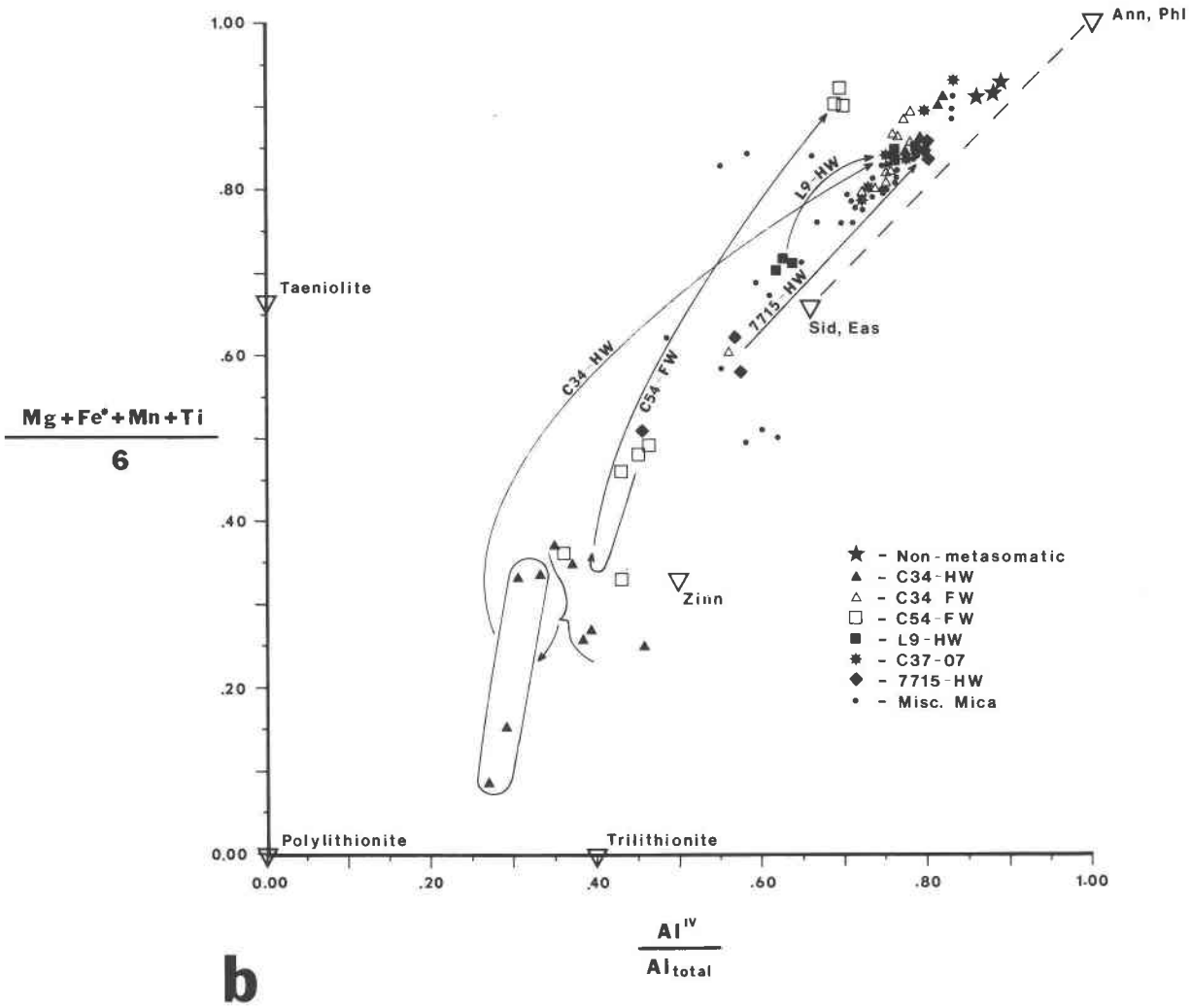

Fig. 5.—*Continued.*

micas, which are nearly identical to those of the hornblendes they replace, fall in the range of magnesian biotites. Biotite near the pegmatite contact, however, deviates markedly from annite-siderophyllite-phlogopite-eastonite solid solutions in having extremely high contents of Rb (≤4.61 wt%), Cs (≤4.98 wt%), F (≤5.88 wt%), and Si [> 6.0 per formula unit (pfu); Table 5], and low contents of ^{IV}Al (Fig. 5a). The nonideal nature of proximal exomorphic micas is also reflected on a plot of the sum of octahedral cations (excluding Li) versus $^{IV}Al/Al_{total}$ (Fig. 5b). Many proximal micas plot near ideal zinnwaldite or approach the trilithionite-polylithionite join on this diagram, suggesting that these micas may have considerable Li contents. This is supported by Li analyses of only a few micas and estimates of Li contents of other samples, which indicate that biotite at the pegmatite contact may contain up to about 1 wt% Li, dropping off to less than 2000 ppm within 1 m of the contact (in lieu of chemical analyses, Li was estimated by difference from microprobe totals: wt% water was estimated by assuming an atom fraction of OH^- pfu = 4 − F pfu and 1 OH^- pfu = approximately 1 wt% water (estimated from Deer et al., 1982)). With increasing distance from the pegmatite, micas approach more typical biotite-phlogopite compositions, much like those of the nonmetasomatic biotite of the unaltered amphibolite (Table 5). The distinction between metasomatic biotite in the alteration aureole and distal, non-metasomatic biotite is reflected not only in composition (i.e., higher rare-alkali and F contents in metasomatic mica; Table 5), but also in grain size and optical properties. Accessory biotite in the unaltered amphibolite is dark brown and usually medium-grained (1–4 mm) and shows

TABLE 5. Electron microprobe analyses of exomorphic trioctahedral micas, averaged with respect to distance from the pegamatite contact

Distance (m):	0.00–0.49	0.50–0.99	1.0–1.99	2.00–2.95	>7.00†
No. of analyses:	178	29	30	26	16
			Oxides (wt%)		
SiO_2	39.35(3.49)	38.34(2.64)	36.19(1.12)	36.11(0.21)	35.52(0.14)
Al_2O_3	17.53(1.57)	16.96(0.27)	17.30(0.61)	17.12(0.30)	16.04(0.17)
MgO	8.03(2.42)	10.63(1.58)	10.21(1.03)	8.32(0.41)	8.88(0.80)
FeO*	16.72(5.72)	15.13(3.42)	19.30(1.83)	22.57(0.89)	23.49(0.16)
TiO_2	0.73(0.49)	1.13(0.15)	1.36(0.21)	1.27(0.27)	2.23(0.18)
MnO	0.26(0.10)	0.22(0.10)	0.19(0.06)	0.12(0.10)	0.18(0.03)
CaO	0.07(0.04)	0.05(0.03)	0.07(0.05)	0.10(0.01)	0.04(0.01)
Na_2O	0.16(0.11)	0.10(0.07)	0.10(0.04)	0.28(0.02)	0.12(0.03)
K_2O	7.73(0.97)	7.85(0.36)	8.35(0.55)	8.54(0.11)	9.13(0.20)
Rb_2O	1.96(1.34)	1.22(1.00)	0.58(0.45)	0.41(0.46)	0.03(0.02)
Cs_2O	1.46(1.44)	1.02(0.73)	0.37(0.11)	0.30(0.31)	0.04(0.02)
F	2.41(1.63)	1.99(1.99)	0.84(0.93)	0.22(0.29)	0.20(0.02)
Total	96.41	94.64	94.86	95.36	95.90
			Cations per 22 oxygens		
Si	6.07(0.19)	5.83(0.26)	5.59(0.15)	5.65(0.09)	5.54(0.04)
^{IV}Al	1.93(0.15)	2.17(0.51)	2.41(0.09)	2.35(0.02)	2.46(0.03)
Tet. sum	8.00	8.00	8.00	8.00	8.00
^{VI}Al	1.26(0.15)	1.57(0.44)	0.74(0.04)	0.89(0.02)	0.51(0.03)
Mg	1.81(0.55)	2.42(0.40)	2.36(0.24)	1.98(0.10)	1.98(0.24)
Fe	2.17(0.81)	1.92(0.48)	2.50(0.29)	3.05(0.17)	3.03(0.02)
Ti	0.11(0.05)	0.13(0.02)	0.16(0.02)	0.17(0.03)	0.26(0.03)
Mn	0.04(0.02)	0.03(0.01)	0.02(0.01)	0.02(0.01)	0.03(0.01)
Sum VI	5.39	6.07	5.78	6.11	5.81
Ca	0.01(0.01)	0.00(0.01)	0.01(0.01)	0.02(0.01)	0.00(0.01)
Na	0.04(0.03)	0.03(0.02)	0.03(0.01)	0.09(0.02)	0.03(0.02)
K	1.51(0.19)	1.52(0.07)	1.65(0.10)	1.64(0.03)	1.82(0.01)
Rb	0.19(0.14)	0.11(0.09)	0.05(0.05)	0.05(0.04)	0.00(0.01)
Cs	0.10(0.09)	0.06(0.04)	0.02(0.01)	0.02(0.01)	0.00(0.01)
Sum XII	1.85	1.70	1.76	1.82	1.85
Total	16.42	16.72	15.95	16.09	15.76
F (pfu)	1.18(0.78)	0.93(0.92)	0.41(0.46)	0.16(0.14)	0.10(0.01)
Mg/(Mg + Fe)	0.45(0.12)	0.56(0.03)	0.48(0.04)	0.39(0.02)	0.39(0.03)
Al/(Al + Si)	0.34(0.02)	0.39(0.06)	0.36(0.01)	0.36(0.01)	0.35(0.01)
K/(K + Rb + Cs)	0.84(0.10)	0.90(0.07)	0.96(0.02)	0.96(0.04)	1.00(0.01)
FI**	7.65(2.13)	5.18(4.24)	3.97(2.81)	1.89(2.60)	0.00(0.10)

† Micas >7.0 m from the contact are not metasomatic in origin. Values in parentheses represent one standard deviation from the mean.

* Total Fe is reported as FeO.

** FI denotes the fluorine index (after Munoz, 1984).

typical birefringence (0.039–0.057). In contrast, biotite produced by K-Rb-Cs-F (± Li) metasomatism is generally fine-grained (0.05–1.0 mm) and shows colorless to pale gray-brown pleochroism and usually lower birefringence (0.033–0.040).

Molar contents of Rb, Cs, and F per formula unit for the metasomatic micas are contoured against distance from the pegmatite contact in Figures 6, 7, and 8, respectively. Note that the contours parallel the shape of the biotite aureole, suggesting that structures near the centers of the sharp peaks above the central ore zone and above and below the western ore zone served as conduits for fluid flow from the pegmatite. Variations in the contents of these elements among proximal biotites at various centers of fluid release also imply that fluids emanating from the pegmatite were not uniform in composition around the deposit. Figure 9 is a plot of the cation total (Rb + Cs) per formula unit of mica versus distance from the pegmatite contact. This plot shows that Rb an Cs contents drop off rapidly with distance from the pegmatite, reach a point of inflection, and then decrease more slowly and approximately linearly out to the limit of the metasomatic biotite halo.

To assess the temperature of K-Rb-Cs-F metasomatism, garnet-biotite geothermometry was performed using adjacent pairs of metasomatic biotite and apparently primary metamorphic garnet from a sample (C37-07) located about 1 m above the pegmatite contact in the hanging wall of the central ore zone. Both biotite and garnet each constituted about 5–10 modal percent of the sample. The biotite has the composition $K_{1.60}(Fe_{2.88}Mg_{2.24})(Al_{1.12}Ti_{0.16})$-$(Si_{5.76}Al_{2.24}O_{20})(OH)_4$ and is relatively poor in rare alkalis (avg.: Rb = 0.06 ± 0.05 wt%; Cs = 0.06 ± 0.06 wt%) and F (avg. = 0.01 ± 0.03 wt%). This biotite plots near primary metamorphic biotite from unaltered amphibolite on Figures 5a and 5b. The garnet rim composition is $Ca_{0.26}$-$(Fe_{2.46}Mg_{0.23}Mn_{0.12})Al_{1.96}Si_{2.97}O_{12}$. Calculated temperatures (matrix biotite–garnet rim, X_{Fe}/X_{Mg} in garnet from 2.43

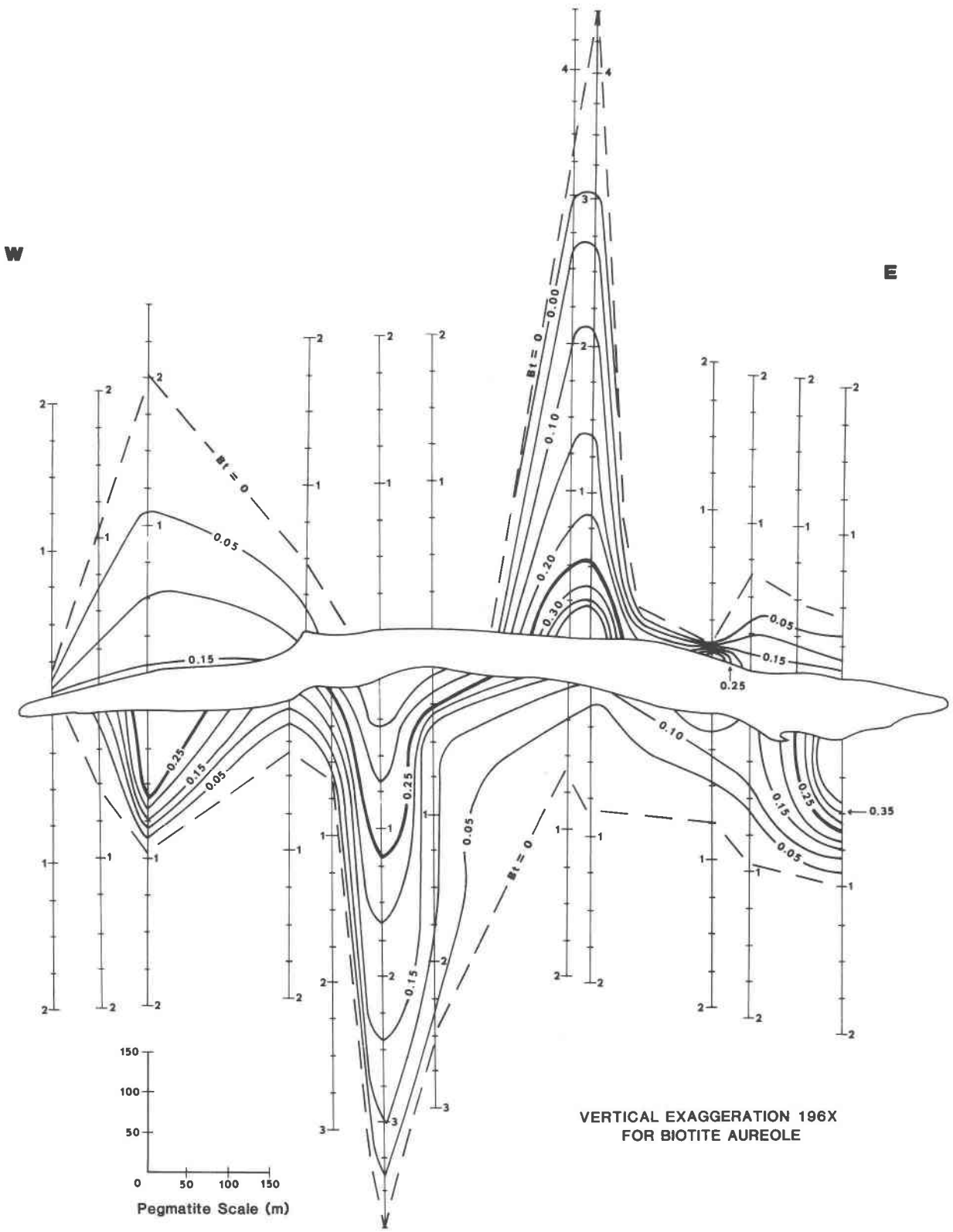

Fig. 6. Contour of the variation in cations of Rb per formula unit of exomorphic biotite from around the Tanco pegmatite.

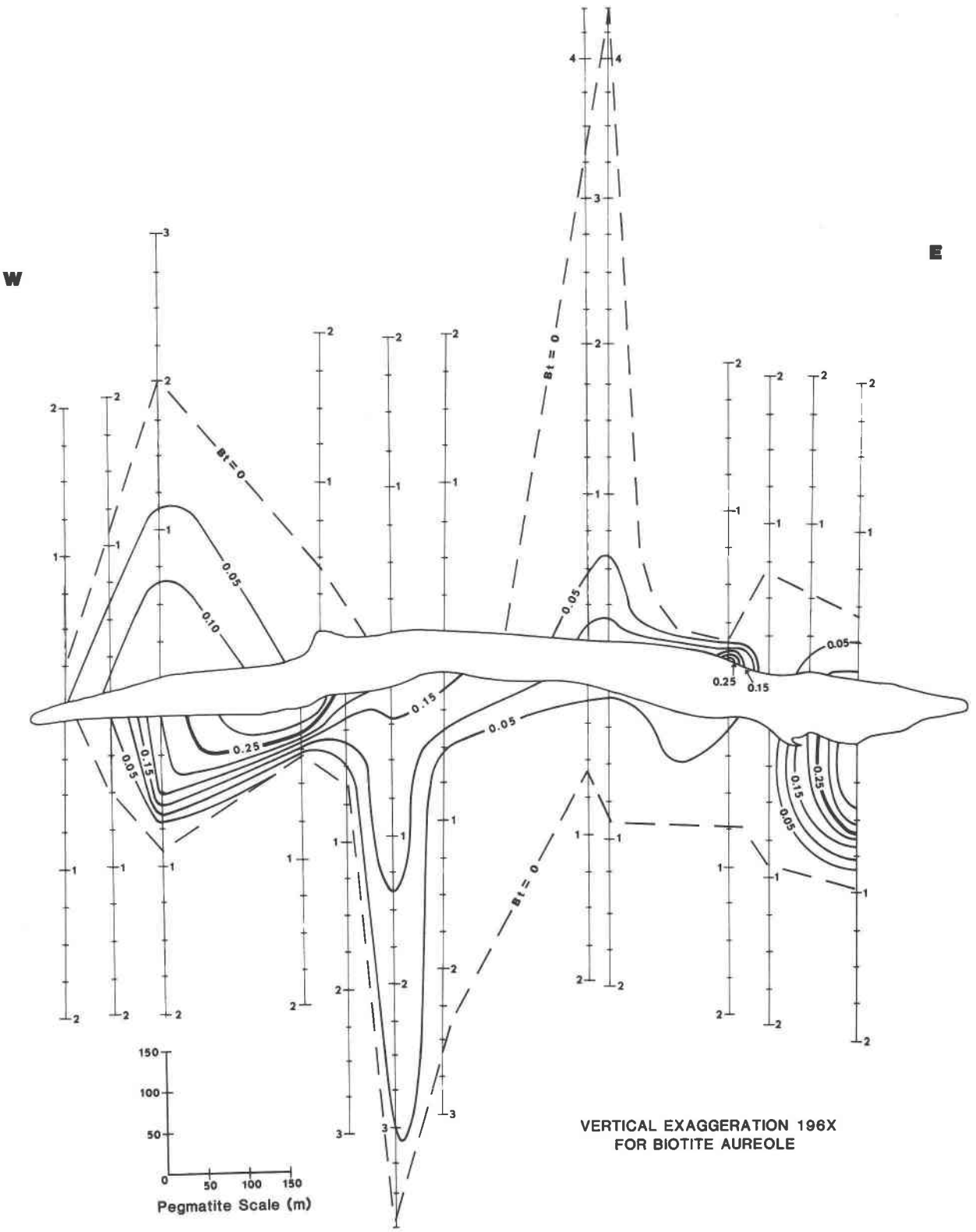

Fig. 7. Contour of the variation in cations of Cs per formula unit of exomorphic biotite from around the Tanco pegmatite.

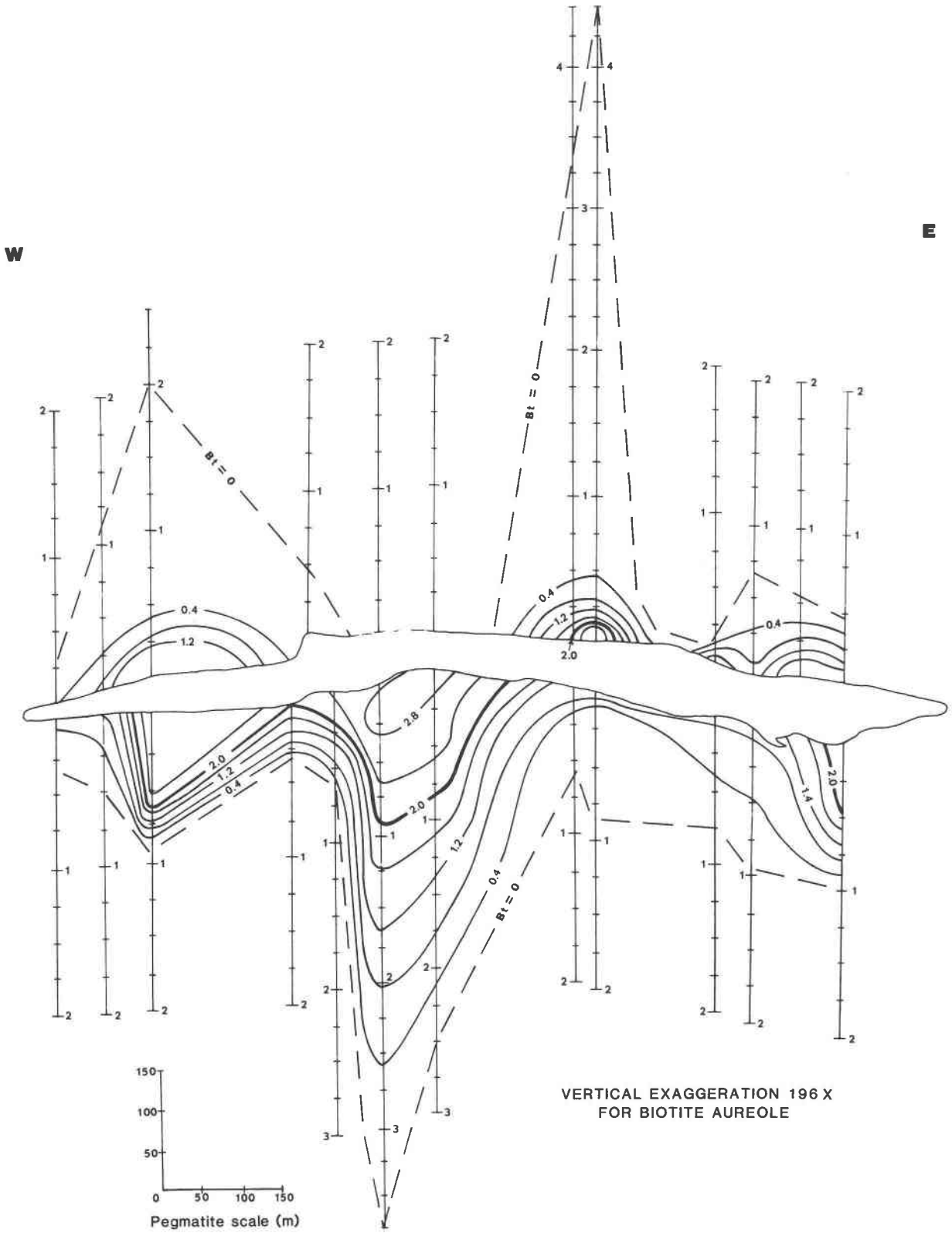

Fig. 8. Contour of the variation in atoms of F per formula unit of exomorphic biotite from around the Tanco pegmatite.

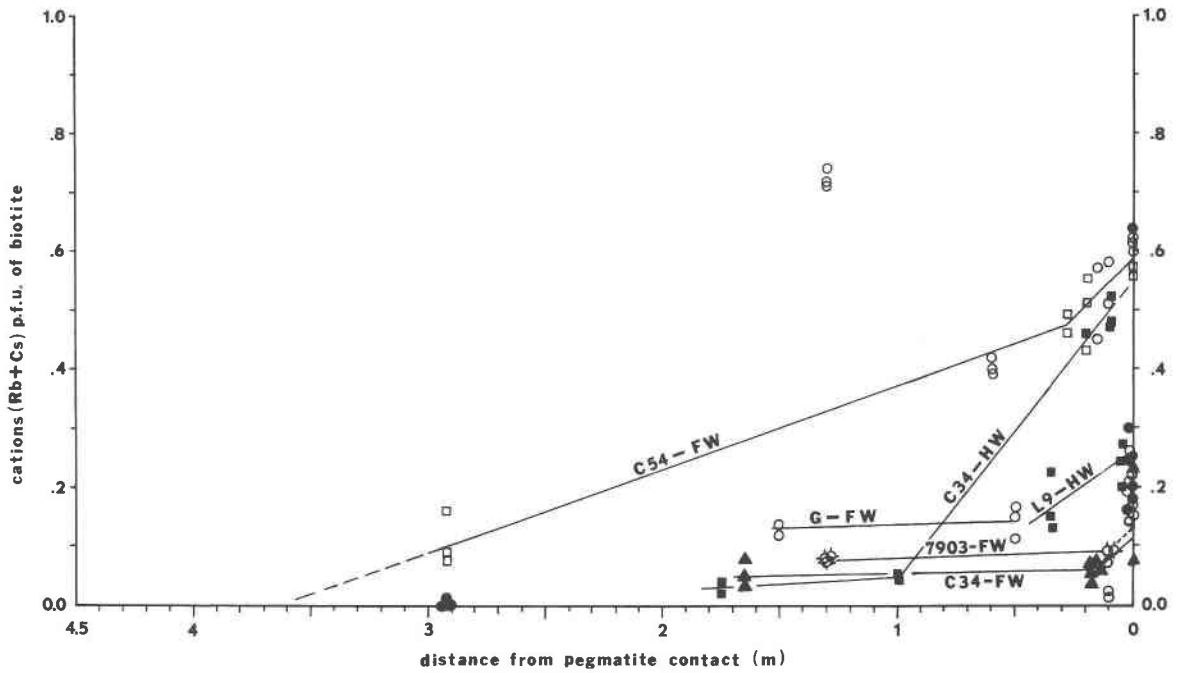

Fig. 9. Cation total (Rb + Cs) per formula unit of exomorphic biotite vs. distance from the Tanco pegmatite. Open symbols indicate footwall samples; closed symbols indicate hanging-wall samples.

to 2.53) using the regular solution model of Indares and Martignole (1985) are in the range 451–458 °C. Apparent equilibration temperatures based on matrix biotite–garnet core compositions (X_{Fe}/X_{Mg} in garnet from 2.61 to 2.78) are near 415 °C; however, if the garnet cores grew during prograde regional metamorphism, they may not have coexisted with biotite.

Apparent fluorine intercepts [IV(F)] and fluorine indices (FI) (Table 5), and log (f_{HF}/f_{H_2O}) for the fluids in equilibrium with these micas (at 400, 500, and 600 °C) were calculated by the methodology of Munoz (1984). Fluorine intercepts and indices can be described as numerical values that express the relative enrichment of F in a mica, assuming compositions within the annite-phlogopite-siderophyllite join. Munoz (1984) defined these functions as $IV(F)_{Bt} = 1.52X_{Mg} + 0.42X_{Ann} + 0.20X_{Sid} - \log(X_F/X_{OH})$ and $FI_{Bt} = 12.8 - 4$ IV(F). Gunow et al. (1980) defined $X_{Sid} = [(3 - Si/Al)/1.75]\,[1 - X_{Mg}]$ and $X_{Ann} = 1 - (X_{Mg} + X_{Sid})$. High fluorine indices denote F-enriched micas. Biotite and sericite from the Henderson molybdenite deposit have FI in the range 9–11.5, and biotite from most porphyry copper deposits is in the range 4–7.5 (Munoz and Gunow, 1982). The apparent fluorine indices for the Tanco exomorphic micas show extreme variation (range: 0.00–11.52; Table 5) and a rapid decrease in FI with distance from the pegmatite contact (Fig. 10).

The apparent fluorine indices of all micas from Tanco cannot be related directly to log (f_{HF}/f_{H_2O}) of the metasomatic fluid, however, because the Tanco micas that contain the most F are also enriched in Li, Rb, and Cs. The fluorine index in biotite is not calibrated to account for Li substitution, and a positive correlation between Li and F contents has been demonstrated in both natural and synthetic biotites (Foster, 1964; Munoz and Ludington, 1974; Munoz and Gunow, 1982; Munoz, 1984). Therefore, the estimation of the true fluorine index of biotite near the Tanco contact is constrained to a high-F, low-Li composition. It is probable that exomorphic biotites with high contents of Rb and Cs also have large contents of Li as well. This is supported by the few Li analyses of proximal biotites (Li = 3250–10 000 ppmw) and the observation that holmquistite is most abundant with biotites that contain the highest (Rb + Cs) and highest fluorine indices. A plot of fluorine index versus cation total of (Rb + Cs) per formula unit in biotite (Fig. 11) shows two distributions (heavy lines): a steeply dipping linear trend at low (Rb + Cs) that intersects a less steeply dipping trend at FI = 5.3 and (Rb + Cs) = 0.1. The points defining the steeply dipping trend correlate with biotites from greater than 0.1–0.3 m from the pegmatite contact (i.e., distal), and, with little overlap, the points from which the upper line was derived (FI > 5.0) correspond to biotites less than 0.35 m from the pegmatite contact. This plot shows that the proximal micas (upper portion of the diagram) have the highest fluorine indices and also contain the highest abundances of Rb, Cs, and, presumably, Li. These variations are emphasized by the trends of micas from individual cores (light lines in Fig. 11). The point where the trends of proximal and distal biotites intersect in Figure 11 (FI = 5.3) corresponds to high-F biotites with minimal rare-alkali contents. The high fluorine indices (FI > 5.3) above this point are believed to result partly from Li (and Rb + Cs?) substitution. On the basis of this interpretation, the fluorine index of 5.3 represents the

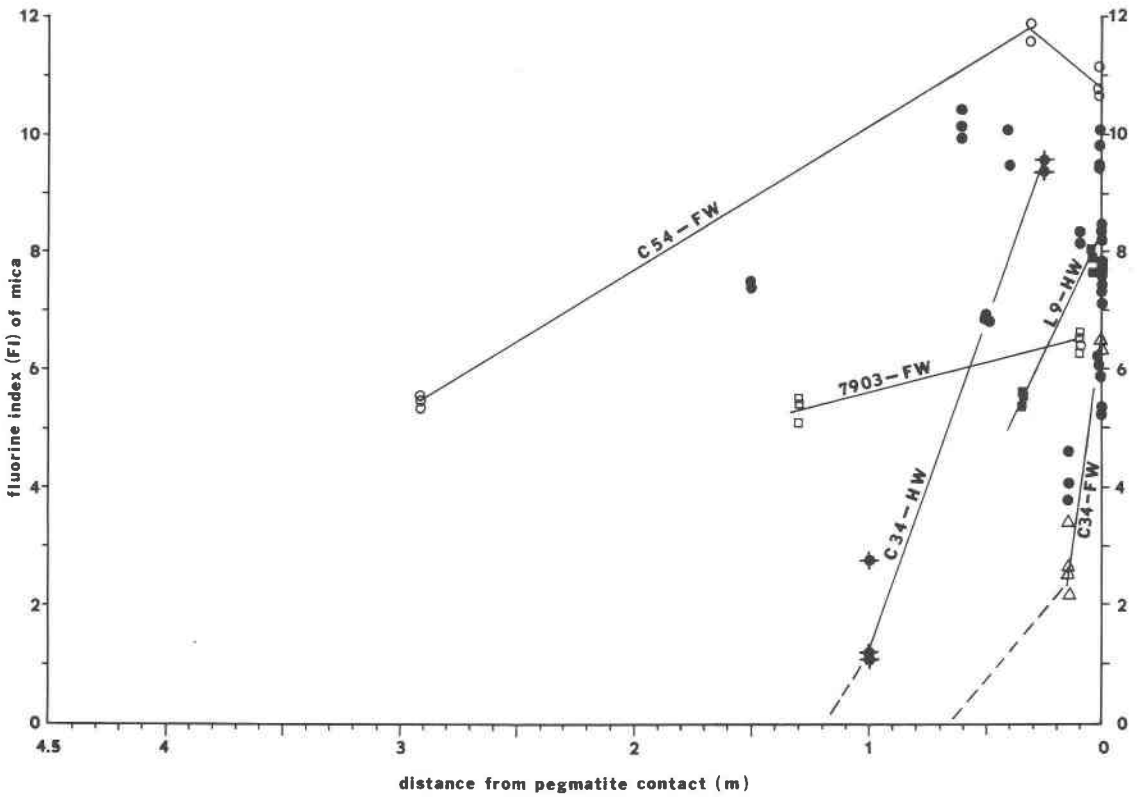

Fig. 10. Fluorine index (FI) of exomorphic biotite (after Munoz, 1984) vs. distance from the pegmatite contact. Open symbols indicate footwall samples; closed symbols indicate hanging-wall samples.

minimum upper limit for micas at the pegmatite contact, because significant quantities of F were consumed by rare-alkali-rich biotite closer to the contact. A value of FI = 5.3 at $T = 451$–458 °C (from garnet-biotite geothermometry) yields $\log(f_{HF}/f_{H_2O}) = -4.9$ for fluids in equilibrium with exomorphic biotite. $\text{Log}(f_{HF}/f_{H_2O})$ calculated for internal pegmatite fluids in equilibrium with primary amblygonite-montebrasite (after Loh and Wise, 1976) with average $X_{amb} = 0.40$ (Černá et al., 1972) is -4.8 at 600 °C and 300 MPa, which agrees well with the value of $\log(f_{HF}/f_{H_2O})$ for fluids equilibrated with exomorphic biotite.

The F contents of biotites correlate positively with Rb + Cs (Figs. 6–11, and Table 5), dropping off rapidly with distance from the pegmatite. The similar trends observed in F, Rb, Cs, and, presumably, Li contents in exomorphic biotite around the pegmatite suggest that both the rare alkalis and F were carried by the same metasomatic fluid. Moreover, these variations also indicate that F and alkalis were depleted from the fluid with increasing distance from the pegmatite. In the hydrothermal conversion of hornblende to biotite by K-rich fluids, the crystal/vapor partition coefficient for K is ≥ 1 (Brimhall et al., 1985). Papike et al. (1983) have demonstrated that biotite is a very effective trap for Rb and Cs. From the observed biotite compositions around Tanco, it appears that nearly all of the K, Li, Rb, Cs, and F lost from the pegmatite during this episode were retained within the exomorphic biotite aureole. Some remobilization of these components from the biotite aureole probably occurred during the ensuing episode of propylitic alteration (chloritization); however, the extent of such alteration is small in comparison to the modal abundance of metasomatic biotite.

Propylitic alteration with concomitant Li and CO_2 influx

Propylitic alteration is by far the most ubiquitous and pervasive alteration type at Tanco, forming a distinct halo 2 to 9 m wide. The propylitic aureole appears to completely surround the pegmatite (Figs. 3 and 4) and encompasses the tourmaline and biotite aureoles. It is characterized by alteration assemblages indicative of greenschist-facies conditions: hornblende → epidote + chlorite + calcite ± titanite ± holmquistite ± oxides; plagioclase → zoisite + clays ± calcite; and biotite → chlorite ± holmquistite. Propylitic alteration is more pervasive and generally penetrates further into the host rock in the hanging-wall than in the footwall amphibolite (Figs. 3 and 4). Additionally, the propylitic assemblage of the hanging wall contains a notably higher modal proportion of calcite than does that of the footwall. All major phases in the propylitic assemblage, including holmquistite (Table 6), are low in Na, K, Rb, Cs, and F.

The association of clay minerals (smectites) with the

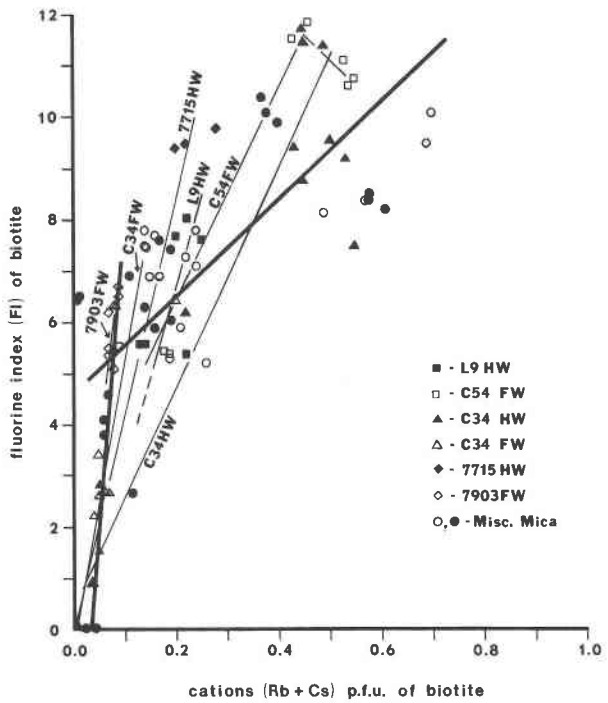

Fig. 11. Fluorine index (FI) vs. the cation total of (Rb + Cs) for exomorphic biotite. Open symbols indicate footwall samples; closed symbols indicate hanging-wall samples.

propylitic assemblage at Tanco indicates that this alteration probably occurred at $T \leq 400$–420 °C (see Velde, 1985). The large quantities of calcite present in pervasively altered wallrock (up to 45 vol%) indicate that the fluids responsible for propylitic alteration were CO_2-rich aqueous solutions. Moreover, the higher abundance of calcite in the hanging-wall assemblage implies that the fluids that invaded the hanging-wall amphibolite were more CO_2 rich than those that invaded the footwall (Morgan and London, 1985; London and Morgan, 1985).

Li exomorphism and holmquistite

Holmquistite is present in all three metasomatic exomorphic assemblages at Tanco. Averaged EMPA of exomorphic holmquistite are listed with associated alteration assemblages in Table 6. The Li contents per formula unit were estimated by difference (assuming full site occupancy), because Li is almost completely ordered at the two octahedral B (M4) sites in holmquistite (Hawthorne, 1981). All Si was assumed to be tetrahedrally coordinated. Where Si < 8 pfu, Al was assigned to fill the remainder of the tetrahedral sites. Al [or Al − (8 − Si) where Si < 8 pfu], Ti, Fe, Mn, and Mg were then assigned to the C (M1, M2, and M3) sites, and any amounts of these cations in excess of 5.00 atoms pfu were subtracted from the 2 B (M4) sites. Finally, Ca was subtracted from the B (M4) sites, yielding the atoms of Li per formula unit.

Although holmquistite displays compositional variability with respect to both major and trace elements, no clear distinction in composition is noted between holmquistite associated with different metasomatic assemblages (Table 6). Holmquistite formed during early metasomatism may have re-equilibrated in part with subsequent and compositionally different pegmatite-derived fluids. In addition, holmquistite and its associated minerals may not represent a single paragenetic assemblage (i.e., multiple generations of holmquistite, each equilibrated with a different pegmatitic fluid, may be superimposed in a given sample).

Relation of wallrock alteration to pegmatite evolution

London (1986a) has presented a model for the internal evolution of the Tanco pegmatite based on studies of pegmatitic fluid inclusions, internal mineral content, and phase-equilibrium experiments in the lithium aluminosilicate system. This model is summarized in Figure 12, and re-evaluated below in light of the new information from wallrock alteration.

Because London's (1986a) model is based on fluid inclusions in spodumene and petalite and on lithium aluminosilicate stabilities, the liquidus temperature and early primary crystallization of the pegmatite remain uncertain prior to petalite saturation in the range 600–700 °C and 3 kbar (point A in Fig. 12). Microthermometric analysis of tourmaline-hosted fluid inclusions led Thomas and Spooner (1987) to propose that the incipient crystallization of the wall zone occurred at approximately 550 °C. This estimate, however, was derived using a pressure correction of 2 kbar. A pressure correction of 3 kbar, which we believe to be more appropriate, would raise this estimate to about 600–650 °C, which falls within the range in which petalite saturation probably occurred (London, 1986a). Early primary crystallization, possibly at slightly higher T, probably included the wall zone, microcline-rich central intermediate zone, and albitite units. Albitites formed throughout the primary crystallization interval (small arrow in Fig. 12). In addition to the voluminous albitites in the eastern ore zone, smaller bodies occur throughout the pegmatite, but especially in the western ore zone where they are associated with the most chemically and mineralogically differentiated assemblages in the pegmatite. Thin bodies of albitite also vein primary microcline and petalite.

Observations from fluid inclusions and phase-equilibrium experiments led London (1986a) to propose that because of high concentrations of Li, B, F, and other incompatible elements in the Tanco system, silicate melt components and H_2O were nearly, if not entirely, miscible during the late stages of primary crystallization. Unequivocal evidence for a low-density vapor phase was found only in secondary fluid inclusions that were entrapped in quartz and spodumene at near-solidus or subsolidus temperatures <470 °C. Wallrock alteration that is clearly pegmatite-related (i.e., the metasomatic events) occurred at $T < 450$–500 °C, as evidenced by geothermometric analysis of metasomatic biotite-garnet pairs, and by the pres-

TABLE 6. Electron-microprobe analyses of holmquistite, averaged with respect to associated exomorphic assemblages

	Tourmaline ± biotite	Biotite	Propylitic assemblage		
				± biotite	± tourmaline
No. of analyses:	5	7	7	10	4
			Oxides (wt%)		
SiO_2	55.38(1.75)	55.11(2.62)	55.64(1.49)	57.58(2.88)	59.05(0.12)
Al_2O_3	12.31(0.29)	12.32(0.97)	12.57(0.18)	12.28(1.41)	12.02(0.06)
MgO	6.11(0.07)	6.62(0.55)	7.38(0.57)	5.42(1.68)	7.20(0.03)
FeO*	17.16(0.44)	18.16(0.68)	15.83(0.62)	18.41(2.89)	15.06(0.02)
TiO_2	0.10(0.02)	0.09(0.01)	0.04(0.04)	0.10(0.03)	0.02(0.01)
MnO	0.25(0.03)	0.25(0.02)	0.16(0.02)	0.17(0.03)	0.13(0.03)
CaO	1.03(0.86)	0.09(0.02)	0.84(0.49)	0.10(0.04)	0.11(0.01)
Na_2O	0.29(0.06)	0.18(0.02)	0.23(0.03)	0.16(0.04)	0.15(0.01)
K_2O	0.15(0.14)	0.08(0.07)	0.05(0.01)	0.01(0.01)	0.01(0.01)
Rb_2O	0.04(0.04)	0.03(0.02)	0.00(0.01)	0.17(0.04)	0.09(0.02)
Cs_2O	0.11(0.10)	0.06(0.05)	0.00(0.01)	0.01(0.02)	0.03(0.03)
F	0.18(0.01)	0.09(0.01)	0.11(0.02)	0.04(0.03)	0.08(0.02)
Total	93.11	93.08	92.85	94.45	93.95
			Cations per 23 oxygens		
Si	7.85(0.17)	7.89(0.21)	7.81(0.15)	8.00(0.16)	8.01(0.02)
^{IV}Al	0.15(0.17)	0.17(0.16)	0.19(0.15)	0.01(0.02)	0.01(0.02)
Tet. sum	8.00	8.06	7.99	8.01	8.02
^{VI}Al	1.96(0.02)	1.97(0.01)	1.97(0.09)	1.91(0.01)	1.99(0.01)
Mg	1.35(0.01)	1.40(0.07)	1.60(0.11)	1.07(0.36)	1.51(0.01)
Fe	2.14(0.08)	2.19(0.02)	1.92(0.08)	2.32(0.42)	1.77(0.01)
Ti	0.01(0.01)	0.01(0.01)	0.01(0.01)	0.01(0.02)	0.01(0.01)
Mn	0.03(0.01)	0.03(0.01)	0.02(0.01)	0.03(0.01)	0.01(0.01)
Oct. sum†	5.49	5.60	5.52	5.34	5.29
Ca	0.16(0.17)	0.01(0.01)	0.13(0.08)	0.01(0.02)	0.02(0.05)
Li‡	1.35(0.27)	1.39(0.43)	1.36(0.17)	1.65(0.23)	1.70(0.25)
Oct. sum† − 5	0.49	0.60	0.52	0.34	0.29
Sum M4	2.00	2.00	2.01	2.00	2.01
Na	0.08(0.02)	0.05(0.01)	0.06(0.02)	0.04(0.02)	0.04(0.03)
K	0.03(0.02)	0.02(0.02)	0.01(0.01)	0.00(0.00)	0.00(0.01)
Rb	0.00(0.01)	0.00(0.01)	0.00(0.01)	0.01(0.01)	0.01(0.01)
Cs	0.01(0.01)	0.00(0.01)	0.00(0.01)	0.00(0.01)	0.00(0.01)
Sum A	0.12	0.07	0.07	0.05	0.05
Total	15.12	15.13	15.07	15.06	15.08
F	0.08(0.01)	0.04(0.04)	0.05(0.01)	0.02(0.01)	0.08(0.01)
Mg/(Mg + Fe)	0.39(0.01)	0.39(0.02)	0.45(0.02)	0.34(0.09)	0.42(0.01)
Al/Si	0.26(0.01)	0.26(0.02)	0.21(0.01)	0.18(0.01)	0.19(0.01)

Note: Values in parentheses represent one standard deviation from the mean.
* Total Fe is reported as FeO.
† Sum of octahedral cations chosen to fill the M1, M2, and M3 sites.
‡ Li per formula unit is estimated by difference; see text.

ence of propylitic alteration associated with each metasomatic event. From the high reactivity of the amphibolite during metasomatism, we infer that influx of any pegmatite-derived aqueous vapor into the wallrocks would be accompanied by metasomatic change. It is also improbable that significant quantities of aqueous vapor built up in the partially crystallized pegmatite prior to wallrock metasomatism. Miarolitic cavities, or collapse structures indicative of former cavities, are virtually nonexistent at Tanco. In total, the record of wallrock alteration is consistent with the model for internal evolution: both lines of evidence suggest that significant quantities of aqueous vapor were generated only as the pegmatite magma approached its solidus over the interval of 470–550 °C (note that Thomas and Spooner, 1985, have proposed that the sequential crystallization of primary albitites, beryl fringe, and quartz bodies ranged from approximately 327 to 265 °C).

The fluid-inclusion study by London (1986a) revealed evidence for a peralkaline, hydrous borosilicate melt or silicate-rich vapor that was present during the crystallization of petalite and spodumene down to 470 °C (points A to C in Fig. 12). The transition from dominantly magmatic to hydrothermal conditions in Tanco was marked by the loss of a lithium tetraborate fluxing component from this late-stage melt and/or silicate-rich aqueous fluid, with the consequent deposition of albite and other silicate and oxide minerals. The only internal units in the Tanco pegmatite that contain any significant amounts of tourmaline are the albitites (in particular the footwall albitites) and wall-zone units. The high contents of lithium tetraborate (diomignite: London et al., 1987b) in spodumene-

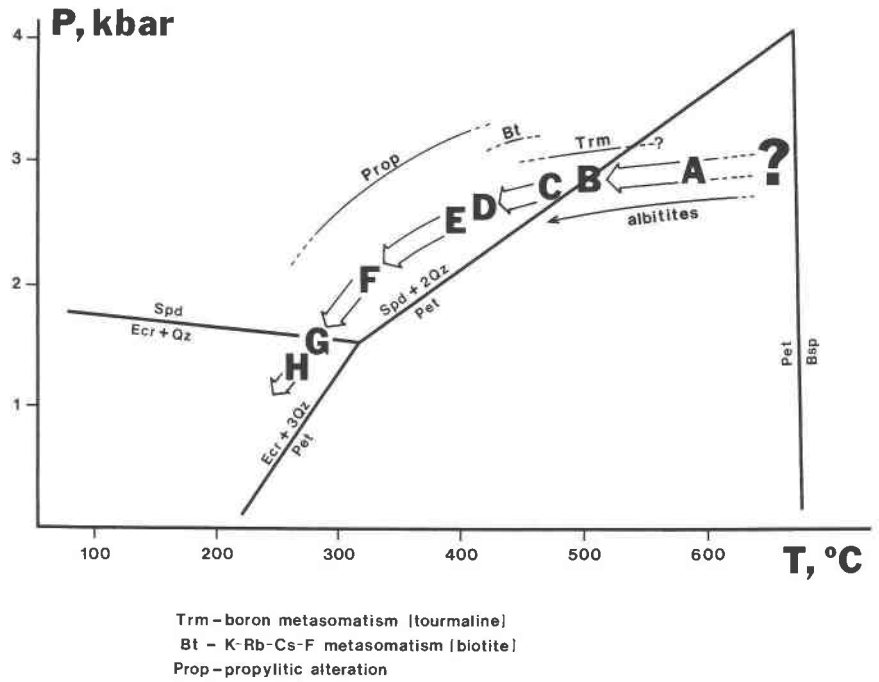

Fig. 12. Evolutionary path for the Tanco pegmatite (wide arrows; from London, 1986a) with correlative representation of wallrock alteration (light lines above evolutionary path). Light arrow indicates trend of increasing chemical fractionation in primary albitite units. Internal crystallization of pegmatite units is discussed in the text. The fluid evolution is summarized as follows: (?–C) Primary crystallization from a dense, hydrous alkali borosilicate fluid. (C–D) Transition of dense, hydrous alkali borosilicate liquid (C) to a solute-poor, CO_2-bearing aqueous solution (D). The composition of the aqueous fluid (in mol%) at the point D is approximately 91% H_2O, 5% CO_2, and 4% NaCl, equivalent. (E) Onset of H_2O-CO_2 liquid immiscibility at a bulk-fluid composition (in mol%) of approximately 80–85% H_2O, 10–15% CO_2, and 5–6% NaCl equivalent. (F) Complete unmixing into separate aqueous and CO_2 fluids. (F–H) Increasing salinity (Na, Mg, Cl, SO_4) in the aqueous fluid signifies the influx of wallrock-derived fluids back into consolidated pegmatite.

hosted fluid inclusions suggest not only that tourmaline crystallization in the wall zone and early albitites was not capable of buffering B activity in the melt or vapor, but also that B was retained within the pegmatite throughout most of the interval of magmatic crystallization. As such, the late, more chemically evolved albitite units may represent the products of B depletion. The process envisioned couples two interactive mechanisms: (1) crystallization of tourmaline leading to melt vesiculation (London, 1986a, 1986c) and (2) further depletion of B from residual melt by preferential partitioning into the vesiculated aqueous vapor ($K_D^{vapor/melt}$ for B $\geq$ 1: Pichavant, 1981; London et al., 1987a). Both H_2O and B lower melt crystallization temperatures; therefore, melt crystallization is driven by a runaway process as the solubility of H_2O in melt is lowered by the progressive loss of B (Pichavant, 1981; London, 1986a, 1986b, 1986c). Unlike many rare-element pegmatites, the Tanco albitites do not contain large quantities of demonstrably late-stage tourmaline. At Tanco, therefore, mechanism 2 in the process may have been principally responsible for the generation of aqueous vapor and the consequent loss of vapor and B to wallrocks. Once the pegmatite system was open to the wallrocks via the exsolved vapor phase, deposition of tourmaline in the wallrocks may have initiated a chemical gradient for continued B loss from the pegmatite; thus, both mechanisms 1 and 2 may have operated at Tanco.

There is a strong spatial correlation between wallrock tourmalinization and the locations of albitite zones within the pegmatite. The spatial, temporal, and compositional evidence indicates that the crystallization of the albitites represents the most probable pegmatitic source of the acidic (?), B-bearing fluids responsible for B metasomatism of the wallrocks. The pervasive tourmaline aureole above the pollucite body in the central ore zone may stem from fluids liberated by primary crystallization of the pollucite body, which probably was among the last pegmatitic zones to crystallize, or from fluids that were liberated from the crystallization of albitite units which passed through (and altered?) the pollucite unit before escaping to the wallrocks.

The probable source of alkalis and F for biotitization of the wallrocks involved sericitic alteration of microcline within the pegmatite. A spatial association of wallrock biotitization with central intermediate zone and mixed zone units has already been noted. Beside the Li-rich mica replacement bodies that were mapped separately as lepidolite units, large quantities of microcline in the central intermediate zone and mixed zone were replaced by sericitic muscovite. Assuming total conservation of alkalis

in the biotite (± holmquistite) alteration aureole, the requisite quantities of K, Rb, and Li for biotitization of amphibolites could have been derived by only 14% sericitization of microcline in the central intermediate zone, mixed zone, and spodumene-quartz units (using microcline compositions from Černý and Macek, 1972). The quantity of Cs consumed by metasomatic biotite would require 31% sericitization of the microcline in these units, or another contribution to the aqueous fluid such as loss from the late-crystallizing pollucite bodies. In the central intermediate zone alone, approximately 70 vol% of the microcline (which initially constituted about 80–90 vol% of the assemblage) shows some degree of replacement by muscovite (P. J. Vanstone, pers. comm., 1985). It is apparent that the sericitic alteration of pegmatitic microcline in the central intermediate zone and mixed zone represents a reservoir capable of supplying the large quantities of alkalis consumed by the formation of metasomatic biotite (see discussion of mass balance, below).

Both the exomorphic biotite near the pegmatite contact and pegmatitic micas (Rinaldi et al., 1972) are enriched in F. This would suggest that the acidic fluids responsible for sericitization of the central intermediate zone were initially rich in F. The spatial association of central intermediate zone and mixed zone units with albitites (both mappable albitite units and small segregations within the central intermediate and mixed zones) and with large exomorphic biotite aureoles suggests that the albitites were likely sources of such F-rich fluids. Moreover, the temperature of K-Rb-Cs-F metasomatism (about 450 °C) is consistent with London's (1986a) estimate of 420–470 °C for crystallization of late-stage albitites and derivation of an acidic aqueous vapor (point C in Fig. 12).

The discrete veining and locally pervasive replacement of metasomatic biotite and tourmaline by chlorite + calcite ± epidote show that propylitic alteration was the latest prevalent type of wallrock alteration. Thus, the pegmatitic aqueous vapor became depleted in B, F, and all alkalis except Li at $T < 450$ °C, after the formation of metasomatic biotite (point D in Fig. 12). London (1986a) showed that the onset of H_2O-CO_2 immiscibility in the pegmatite occurred at about 390 °C and 250 MPa (point E in Fig. 12), continuing toward complete unmixing at about 300 °C and 220 MPa (point F in Fig. 12). Such unmixing and upward escape of a comparatively low-density CO_2 fluid would account for the much higher modal abundance of calcite (up to 45 vol%) in the hanging-wall propylitic assemblage.

The widespread distribution and association of holmquistite with all three metasomatic assemblages at Tanco suggests that Li was released continuously during the hydrothermal stage of the pegmatite and had multiple pegmatitic sources. The association of holmquistite with B metasomatism may signify that Li was also liberated during the crystallization of pegmatitic albitites and spodumene (petalite)–quartz units, which follows from the loss of the $Li_2B_4O_7$ component from the borosilicate melt or vapor phase (London, 1986a).

The P-T path below point F in Figure 12 is characterized by increasing salinity in aqueous fluids within the pegmatite. The fluids in this P-T interval record increasing Mg, Ca, and Cl contents, occasionally manifested as daughter minerals of epsomite, halite, and calcite in the sequentially latest secondary fluid inclusions hosted by quartz (London, 1986a). We believe that this change in fluid-inclusion chemistry reflects an influx of wallrock-derived fluid back into the crystallized pegmatite. By this stage of the pegmatite's evolution, metasomatic alteration of the wallrocks was essentially complete.

Utility of wallrock alteration as a guide to pegmatite exploration

Figures 3 and 4 show that the metasomatic halos are narrow (≤9.0 m) in comparison to the size of the deposit and that the distribution of metasomatic alteration is sporadic and heterogeneous around the Tanco pegmatite. Moreover, rare-alkali-rich metasomatic phases are absent at a distance of more than about 4.5 m from the pegmatite. These characteristics indicate that wallrock alteration may be of only marginal value in the exploration for hidden pegmatites, even large ones such as Tanco. Detection of rare-alkali dispersion halos by whole-rock geochemical sampling (e.g., Beus, 1961; Ovchinnikov and Solodov, 1971; Ovchinnikov, 1976; Trueman, 1978; Trueman and Černý, 1982) remains a more effective way of locating buried rare-element pegmatites. Among the metasomatic minerals in the Tanco alteration aureole, holmquistite is the most ubiquitous phase. The association of holmquistite with highly differentiated, usually large rare-element pegmatites may be useful for assessment of the economic potential of a known pegmatite body (e.g., Hornung, 1962; Heinrich, 1965; Glebov and Khlebnikova, 1973; Trueman and Černý, 1982; London and Burt, 1982b; London, 1984a, 1986b).

At Tanco, tourmalinized wallrock may reflect the presence of adjacent Be- and/or Ta-mineralized albitites. Aureoles of metasomatic biotite correlate with sericitized (and in some cases Ta-mineralized) microcline units. Altered wallrocks where holmquistite is the only, or predominant, rare alkali–bearing metasomatic phase are developed near large lithium aluminosilicate bodies. These correlations may be useful in conjunction with core-drilling programs. Because of the extremely coarse grain size of primary pegmatitic minerals, a particular drill hole may intersect relatively few crystals, which may or may not be indicative of the predominant mineral assemblage of the pegmatitic zones. Wallrock metasomatism, therefore, provides an indication of the predominant, or average, mineral content of the adjacent pegmatite.

Pegmatite-wallrock mass balance

In an effort to examine the mass balance of components between wallrocks and pegmatite, the molar quantites of K, Rb, Cs, Li, B, and F consumed by exomorphic phases were compared to the composition of the pegmatite for which we had adequate control (cross-hatched area in Fig.

2). It should be noted that the following discussion of mass balance is intended to consider only this portion of the pegmatite. The pegmatite composition was estimated by (1) determining the volume of each internal unit by examining the areas of vertical cross sections spaced 50 ft (~15 m) apart, which were derived from isopach maps of each internal zone at a scale of 1:1200; (2) converting total volumes of internal units into mineral volumes using modes (Table 1) estimated from Crouse and Černý (1972) an Černý (1982a) and modified by our own observations; (3) conversion of mineral volumes into moles through division by molar volumes; and (4) conversion of moles of minerals into moles of elements based on representative mineral compositions (Foord, 1972; Moore, 1982; Černá et al., 1972; Černý and Macek, 1972; Grice et al., 1972; Rinaldi et al., 1972).

The molar abundances of K, Rb, Cs, Li, B, F, and CO_2 in the wallrocks were estimated by correlating the modal abundance of metasomatic phases with their compositions. Modal volumes of exomorphic phases were determined by examining "modal shells" of each phase in the wallrocks within the metasomatic halo. The total volumes of metasomatic tourmaline, biotite, and holmquistite were then converted to masses through mineral densities (Trm = 3.15 g/cm^3; Bt = 2.7–3.3 g/cm^3; Hlm = 3.05 g/cm^3). The total masses were then converted to moles through division by molar masses (g.f.w.) of exomorphic phases at Tanco, based on the observed mineral compositions. The molar abundance of pegmatite-derived CO_2 was based on the molar abundance of metasomatic calcite. Carbonate-rich wallrock samples stained with alizarin red show that exomorphic carbonates are strongly dominated by calcite (>95 vol%) as opposed to dolomite. The molar abundance of metasomatic calcite was determined by division of the modal volume (derived as above) by its molar volume (36.934 cm^3/mol).

Boron

Total molar quantities of B were derived from the modal abundance and compositions of exomorphic and pegmatitic tourmalines, plus an additional estimated reservoir of 500 ppmw B in pegmatitic spodumene (qualitative ion-microprobe analyses by Erik Steele, National Bureau of Standards, Gaithersburg, Maryland, U.S.A.). The minimum estimate of the abundance of exomorphic tourmaline is about 5×10^8 mol. From this estimate, about 10^9 mol of B, 10^8 mol of F, and 10^7 mol of Li (excluding holmquistite) were consumed by metasomatic tourmaline. The uncertainty associated with these calculations is difficult to assess, because the grid for wallrock sampling is wide with respect to changes in zonation within the pegmatite. This estimate of B loss is significant, however, because it represents at least 46% of the original B content of the pegmatite magma. On a volumetric basis, 10^9 mol of B represents a mass flux out of the pegmatite of about 103 mol of B per cubic meter of consolidated pegmatite.

We believe that the value of 10^9 mol of B underestimates the actual amount of B introduced to the wallrocks for two reasons. First, the thickest and most extensive aureole of tourmalinization beneath the albitites in the eastern ore zone expands to the east, where no wallrock samples are available. Second, reconnaissance hydrothermal tourmalinization experiments using an unaltered amphibolite (App. 1) indicate that the formation of metasomatic tourmaline occurs only in solutions with low pH (i.e., with acid rather than alkaline B sources). The results suggest that the amount of tourmaline recorded by amphibolitic host rocks may be a function of the proportion of acidic/alkaline borate species in the pegmatite-derived aqueous fluid. The presence of late-stage, peralkaline borosilicate melt (London, 1986a), the occurrence of crystalline $Li_2B_4O_7$ at Tanco (London et al., 1987b), and the association of holmquistite with metasomatic tourmaline (indicating Li + B influx) imply that a significant proportion of B in exsolved aqueous fluid may have existed as a peralkaline borate species, which apparently does not promote tourmalinization of amphibolitic wallrocks.

Alkalis

By correlating the molar abundance of biotite with its composition (from analyses), it is estimated that approximately 10^8 mol of K, 10^8 mol of Rb, 10^7 mol of Cs, 10^6 mol of Li (excluding holmquistite), and 10^8 mole of F were incorporated in the wallrocks during K-Rb-Cs-F (± Li) metasomatism. The uncertainties associated with estimation of biotite abundance between sample points is minimized by the strong positive correlation of exomorphic biotite with internal central intermediate zone and mixed zone units, which are well located. The molar estimates of alkalis incorporated in biotite are regarded as minimum values, because some biotite was destroyed during subsequent propylitic alteration. Trueman (1978) has noted whole-rock anomalies in Li and Rb up to 180 ppmw within 15 m above the central ore zone, decreasing to less than 30 ppmw at 92 m above the western ore zone. Li and Rb could have been dispersed into apparently unaltered amphibolites by fluids that gained rare alkalis during propylitic alteration of biotite. The estimates of K, Rb, and Cs loss represent about 4%, 6%, and 13% of their respective molar quantities in the original pegmatite magma. These values correlate to mass fluxes of about 50, 10, and 5 mol of K, Rb, and Cs per cubic meter of pegmatite. Moreover, the estimated quantities of K, Rb, and Li associated with the formation of metasomatic biotite represent only 5%, 9%, and 4% of their respective abundances currently residing in microcline within the central intermediate, spodumene-quartz, and mixed pegmatite zones. This suggests that less than 14% sericitization of microcline could have provided an adequate source of alkalis for this metasomatic event. The observation that Cs consumption by the wallrocks represents about 48% of that preserved in pegmatitic microcline may signify that crystal/vapor distribution coefficients for Cs were much lower than for the other alkalis, or that Cs may have an additional pegmatitic source (e.g., the pollucite units).

Based on the modal abundance of holmquistite and an

estimated average Li content of 1.5 atoms per formula unit, approximately 10^8 mol of Li were trapped in the wallrocks in the form of holmquistite. In total from all metasomatic phases, approximately 3×10^8 mol of Li were lost to the wallrocks. This represents about 2% of the original Li content in this portion of the pegmatite, or a mass flux of about 31 mol Li per cubic meter of pegmatite.

In contrast to Li, K, Rb, and Cs, which are largely conserved in the altered amphibolite, there are no metasomatic phases that record an influx of Na from pegmatite to wallrocks. Plagioclase in the host amphibolite could have contributed the minor quantities of Na in tourmaline. Relic plagioclase in the recrystallized amphibolite shows no evidence of Na enrichment (in fact, shows lower Ab content compared to distal amphibolite), and secondary albite is not present in the retrograde propylitic alteration assemblages. A Cl- or F-bearing aqueous fluid in or near equilibrium with alkali feldspars at 450–550 °C would have contained significant quantities of Na, with $X_{Na/(Na+K)}$ approximately = 0.8 (Orville, 1963; Barton and Franz, 1983). In view of the large quantities of K trapped in metasomatic biotite, it is probable that even greater molar masses of Na were lost from the pegmatite without conservation in the wallrocks. We have examined metasomatic phases in the altered wallrocks for halite-saturated inclusions, but have found no inclusions suitable for study. An additional indication of Na loss is the low Na_2O/K_2O weight ratio (0.63) calculated from the modal mineral abundances of the pegmatite. This alkali ratio, which is >1 in other rare-element pegmatites (e.g., Harding: Burnham and Jahns, 1962), suggests the possibility that much of the sericitic muscovite within Tanco may have replaced plagioclase rather than microcline.

Fluorine

From all metasomatic phases, a total of slightly less than 10^9 mol of F was lost from the pegmatite. This represents about 14% of the estimated F content of this portion of the pegmatite, or a mass flux of about 75 mol of F per cubic meter of pegmatite. The uncertainties associated with this estimate are especially high, because the pegmatitic sources for F are not well defined, and in particular, the modal abundance of amblygonite-montebrasite is not known with as much certainty as the other important phases in the pegmatite mode.

CO_2 and H_2O

The molar abundance of metasomatic calcite in the wallrocks records the absorption of about 4×10^8 mol of CO_2. This figure probably underestimates the actual pegmatitic loss because it assumes total conservation of CO_2 in the exomorphic aureole. Additional uncertainties, which may partly offset this underestimation, include the unknown X_{CO_2} in connate fluids prior to metasomatism, and a small (avg. $\ll$1 vol%) calcite content in the unaltered amphibolite. Assuming conservation of CO_2 in the exomorphic aureole, the estimate of 4×10^8 mol correlates with a mass flux of about 45 mol of CO_2 per cubic meter of pegmatite, or slightly less than 0.1 wt% of the original pegmatite magma.

From fluid-inclusion data, London (1986a) ascertained that vapor exsolved within the pegmatite between 400 and 450 °C contained 10–15 mol% CO_2. On the basis of calcite (CO_2) abundance, this would correspond to 2.5×10^9 to 4.0×10^9 mol of H_2O introduced during propylitic alteration of the wallrocks. An additional 2.5×10^9 mol of H_2O was consumed by hydration during the formation of metasomatic tourmaline and biotite, giving a minimum total quantity of 5.0×10^9 to 6.5×10^9 mol of pegmatite-derived H_2O. This mass of H_2O corresponds to approximately 0.45 wt% of the total pegmatite mass, which itself contains <1 wt% H_2O in hydrous phases. Clearly, then, pegmatite-derived H_2O was not conserved during wallrock alteration.

Conclusions

The amphibolites surrounding the Tanco pegmatite were very reactive to pegmatite-derived fluids and hence constitute a useful monitor of pegmatite fluid evolution. The type of metasomatic wallrock alteration around Tanco generally reflects the dominant minerals of proximal internal pegmatite units, and also documents major changes in bulk-fluid chemistry (e.g., H_2O-CO_2 immiscibility). The three-dimensional shapes of alteration aureoles, however, are controlled largely by inherited host-rock structures and vary with location around the deposit. All metasomatic aureoles around Tanco are narrow with respect to the dimensions of the pegmatite and hence would be of little use in blind exploration. The alteration minerals, however, may be combined with drilling data to better define the nature and extent of potential ore units.

The chemistry and sequence of wallrock metasomatism are entirely consistent with the recently developed model for internal evolution of the Tanco deposit (London, 1986a). Both lines of evidence indicate that large quantities of aqueous vapor were generated in the pegmatite at T < 500–550 °C, near the magmatic-hydrothermal transition. There is no evidence that the pegmatite attained early saturation in a "typical," mobile aqueous vapor phase. The generation of an acidic B- and F-rich fluid from crystallization of albitites and the consequent sericitic alteration of adjacent microcline- and spodumene-rich zones correlate in time, temperature, and sequence with tourmalinization of the wallrocks, followed by the biotite-forming metasomatic event. A higher abundance of calcite in the propylitic aureole of the hanging-wall amphibolite also correlates with unmixing of H_2O and CO_2 fluids within the pegmatite.

One of the most important results of this study is that enormous quantities of alkalis, F, and especially B have been lost from the pegmatite. Although pegmatite-derived Li, K, Rb, Cs, and F may have been largely conserved in the altered amphibolite, all B, and certainly Na were not. The concentration and subsequent loss of B and F from late-stage pegmatite melt stems from the inability of com-

mon pegmatite minerals to buffer the concentrations of these components at low values (London, 1986a, 1986c, 1986d, 1987). In addition, the pegmatite composition is more aluminous than the original pegmatite magma, because about 10^9 mol of alkalis was lost to the wallrocks. For this reason, chip composites of rare-element pegmatites probably do not represent actual magma compositions (e.g., see London, 1986d), especially with regard to the geochemically important rare alkalis, B, and F.

Acknowledgments

This study was supported by grants to D.L. from the U.S. Bureau of Mines (Allotment Grant G1164140), the National Science Foundation (EAR-8516753), and the University of Oklahoma Research Council. Graduate research grants to G.B.M. were provided by the Geological Society of America and Sigma Xi, the Scientific Research Society of America. We are grateful to the Tantalum Mining Corporation of Canada Ltd. for access to wallrock core and geologic cross sections of the Tanco mine. We thank Petr Černý and Peter Vanstone for valuable discussions and Don Burt and Chip Shearer for thoughtful reviews of the manuscript. Thanks also to Robin Springer for his assistance in the thin-section lab, to Dwight Deuring for his help on the microprobe, and to Kevin Crowley for his assistance with mica separations.

Appendix 1: Tourmalinization experiments

Reconnaissance tourmalinization experiments were carried out using a fine-grained, unaltered amphibolite from core 7823 as starting material. The starting amphibolite was finely ground (−200 mesh) and loaded into Au capsules with boric acid (H_3BO_3) and sodium tetraborate decahydrate ($Na_2B_4O_7 \cdot 10H_2O$) as B sources in separate experiments. About 25 wt% of a B source and 25 wt% distilled and deionized water were added to each charge to insure saturation of both components. Experiments were conducted in water-pressurized, cold-seal reaction vessels, and charges were run at 600 °C and 200 MPa for 9 d. Temperature was measured with internal Chromel-Alumel thermocouples (total uncertainty = ±4 °C), and pressure was monitored with a Heise Bourdon tube gauge open to the experiments and a pressure buffer (uncertainty <10 MPa).

The first series of experiments were not seeded with tourmaline, in order to simulate the introduction of B-rich aqueous fluid to tourmaline-absent amphibolite host rocks. Replicate experiments seeded with schorl yielded identical results. In both cases, approximately 60–70 vol% of the amphibolite charges using boric acid as the B source were replaced by tourmaline that is compositionally similar to tourmaline from the Tanco wallrocks. The experiments using sodium tetraborate as the B source failed to produce tourmaline; these experiments yielded a more sodic hornblende that coexisted with an Na-enriched plagioclase and a B-rich melt (anorthite-albite-danburite-reedmergerite solid solution). Tourmaline seed crystals in the sodium borate experiments showed extensive dissolution.

In addition to amphibolite, similar experiments were conducted using muscovite and muscovite + albite assemblages, with and without tourmaline seed crystals. In all cases, tourmaline failed to grow in any experiments using H_3BO_3 or $Na_2B_4O_7$, and tourmaline seed crystals in all runs dissolved nearly to completion.

References cited

Bailey, S.W. (1984) Classification and structures of the micas. Mineralogical Society of America Reviews in Mineralogy, 13, 1–12.

Barton, M.D., and Franz, J.D. (1983) Exchange equilibria of alkali feldspars with fluoride-bearing fluids. Carnegie Institution of Washington Year Book 82, 377–381.

Bence, A.E., and Albee, A.L. (1968) Empirical correction factors for the electron microanalysis of silicates and oxides. Journal of Geology, 76, 382–403.

Beus, A.A. (1961) Wallrock alterations of hydrothermal-pneumatolitic deposits of rare elements. Sovietskaya Geologiya, 4, 114–126 (in Russian; not seen) [transl. in International Geological Review, 4, 1144–1153].

Brimhall, G.H., Agee, Carl, and Stoffregen, Roger (1985) The hydrothermal conversion of hornblende to biotite. Canadian Mineralogist, 23, 369–379.

Brisbin, W.C., and Trueman, D.L. (1982) Dilation mechanics of fractures during pegmatite emplacement, Winnipeg River area, Manitoba. Mineralogical Association of Canada Programs with Abstracts, 7, 40.

Burnham, C.W., and Jahns, R.H. (1962) A method for determining the solubility of water in silicate melts. American Journal of Science, 260, 721–745.

Černá, Iva, Černý, Petr, and Ferguson, R.B. (1972) The Tanco pegmatite at Bernic Lake, Manitoba. III. Amblygonite-montebrasite. Canadian Mineralogist, 11, 643–659.

Černý, Petr. (1982a) The Tanco pegmatite at Bernic Lake, southeastern Manitoba. Mineralogical Association of Canada Short Course Handbook 8, 527–543.

——— (1982b) Anatomy and classification of granitic pegmatites. Mineralogical Association of Canada Short Course Handbook 8, 1–39.

Černý, Petr, and Macek, Josef. (1972) The Tanco pegmatite at Bernic Lake, Manitoba, V. Colored potassium feldspars. Canadian Mineralogist, 11, 679–689.

Černý, Petr, Meintzer, R.E., and Anderson, A.J. (1985) Extreme fractionation in rare-element pegmatites: Selected examples of data and mechanisms. Canadian Mineralogist, 23, 381–421.

Crouse, R.A., and Černý, Petr. (1972) The Tanco pegmatite at Bernic Lake, Manitoba. I. Geology and paragenesis. Canadian Mineralogist, 11, 591–608.

Deer, W.A., Howie, R.A., and Zussman, J. (1982) An introduction to the rock-forming minerals. Wiley, Essex, Great Britain.

Donnay, G., and Buerger, M.J. (1950) The determination of the crystal structure of tourmaline. Acta Crystallographica, 3, 379–388.

Engel, A.E.J., and Engel, C.G. (1962) Hornblendes formed during the progressive metamorphism of amphibolites, northwest Adirondak Mountains, New York. Geological Society of America Bulletin, 73, 1499–1514.

Foit, F.F., and Rosenberg, P.E. (1979) The structure of vanadium-bearing tourmaline and its implications regarding tourmaline solid solutions. American Mineralogist, 64, 788–798.

Foord, E.E. (1972) Minerals of tin, titaniaum, niobium, and tantalium in granitic pegmatites. Mineralogical Association of Canada Short Course Handbook 8, 187–238.

Foster, M.D. (1964) Water contents of micas and chlorites. U.S. Geological Survey Professional Paper 474-F.

Glebov, M.P., and Khlebnikova, A.A. (1973) Holmquistite in the haloes of rare-metal pegmatites. Vaprosy Mineralogii Geokhimii Mestorozhdenii Vostochnoi Sibiri, 51–57 (in Russian; not seen) [transl. abs. in Chemical Abstracts (1973), 83, #13389x].

Grice, J.D., Černý, Petr, and Ferguson, R.B. (1972) The Tanco pegmatite at Bernic Lake, Manitoba. II. Wodginite, tantalite, pseudo-ixiolite, and related minerals. Canadian Mineralogist, 11, 609–642.

Gunow, A.J., Ludington, S.D., and Munox, J.L. (1980) Fluorine in the micas from the Henderson molybdenite deposit, Colorado. Economic Geology, 75, 1127–1137.

Hawthorne, F.C. (1981) Crystal chemistry of the amphiboles. Mineralogical Society of America Reviews in Mineralogy, 9A, 1–102.

Hawthorne, F.C., and Černý, Petr. (1982) The mica group. Mineralogical Association of Canada Short Course Handbook 8, 63–98.

Heinrich, E.W. (1965) Holmquistite and pegmatitic lithium exomorphism. Indian Mineralogist, 6, 1–13.

Hornung, G. (1962) Wall rock composition as a guide to pegmatite mineralization. Economic Geology, 57, 1127–1130.

Hutchinson, R.W. (1959) Geology of the Montgary pegmatite. Economic Geology, 54, 1525–1542.

Indares, A., and Martignole, J. (1985) Biotite-garnet geothermometry in the granulite facies: The influence of Ti and Al in biotite. American Mineralogist, 70, 272–278.

Jahns, R.H. (1982) Internal evolution of pegmatite bodies. Mineralogical Association of Canada Short Course Handbook 8, 292–327.

Jahns, R.H., and Burnham, C.W. (1969) Experimental studies of pegmatite genesis: I. A model for the derivation and crystallization of granitic pegmatites. Economic Geology, 64, 843–864.

Leake, B.E. (1965) The relationship between composition of calciferous amphibole and grade of metamorphism. In W.S. Pitcher, and G.W. Flinn, Eds., Controls of metamorphism, p. 299–318. Wiley, New York.

——— (1968) Catalogue of analyzed calciferous and subcalciferous amphiboles together with their nomenclature and associated minerals. Geological Society of America Special Paper 98.

Loh, S.E., and Wise, W.S. (1976) Synthesis and fluorine-hydroxl exchange in the amblygonite series. Canadian Mineralogist, 14, 357–363.

London, David. (1982) Fluid-solid inclusions in spodumene from the Tanco pegmatite, Bernic Lake, Manitoba. Geological Society of America Abstracts with Programs, 14, 549.

——— (1984a) Holmquistite, tourmaline, and wallrock alteration around rare-metal pegmatites (abs.). EOS, 65, 1124.

——— (1984b) Experimental phase equilibria in the system $LiAlSiO_4$-SiO_2-H_2O: A petrogenetic grid for lithium-rich pegmatites. American Mineralogist, 69, 995–1004.

——— (1985) Origin and significance of inclusions in quartz: A cautionary example from the Tanco pegmatite, Manitoba. Economic Geology, 80, 1988–1995.

——— (1986a) The magmatic-hydrothermal transition in the Tanco pegmatite: Evidence from fluid inclusions and phase equilibrium experiments. American Mineralogist, 71, 376–395.

——— (1986b) Holmquistite as a guide to pegmatitic rare metal deposits. Economic Geology, 81, 704–712.

——— (1986c) Formation of tourmaline-rich gem pockets in miarolitic pegmatites. American Mineralogist, 71, 396–405.

——— (1986d) Petrogenesis of rare-element pegmatites: Evidence from fluid inclusions and phase equilibrium experiments. International Mineralogical Association Abstracts with Program, 159.

——— (1987) Internal differentiation of rare-element pegmatites: The effects of boron, phosphorus, and fluorine. Geochimica et Cosmochimica Acta, 51, 403–420.

London, David, and Burt, D.L. (1982a) Chemical models for lithium aluminosilicate stabilities in pegmatites and granites. American Mineralogist, 67, 494–509.

——— (1982b) Lithium minerals in pegmatites. Mineralogical Association of Canada Short Course Handbook 8, 99–133.

London, David, and Morgan, G.B., VI. (1985) Wallrock alteration around the Tanco rare-element pegmatite, Manitoba: Relations to pegmatite evolution (abs.). EOS, 66, 1154.

London, David, Morgan, G.B., VI, and Hervig, R.L. (1987a) Element partitioning and fractionation trends in volatile- and LILE-rich rhyolite (abs.). EOS, 68, 450.

London, David, Zolensky, M.E., and Roedder, Edwin. (1987b) Diomignite: Natural $Li_2B_4O_7$ from the Tanco pegmatite, Manitoba. Canadian Mineralogist, 25, 173–180.

Moody, J.B., Meyer, D., and Jenkins, J.E. (1983) Experimental characterization of the greenschist/amphibolite boundary in mafic systems. American Journal of Science, 283, 48–92.

Moore, P.B. (1982) Pegmatite minerals of P(V) and B(III). Mineralogical Association of Canada Short Course Handbook 8, 267–291.

Morgan, G.B., VI, and London, David. (1985) Wallrock alteration around the Tanco rare-element pegamtite, Manitoba: Petrology of alteration halos (abs.). EOS, 66, 1153–1154.

Munoz, J.L. (1984) F-OH and Cl-OH exchange in micas with applications to hydrothermal ore deposits. Mineralogical Association of America Reviews in Mineralogy, 13, 469–493.

Munoz, J.L., and Gunow, A. (1982) Fluorine index: A simple guide to high fluorine environments (abs.). Geological Society of America Abstracts with Programs, 14, 573.

Munoz, J.L., and Ludington, S.D. (1974) Fluoride-hydroxyl exchange in biotite. American Journal of Science, 274, 396–413.

Norton, J.J. (1983) Sequence of mineral assemblages in differentiated granitic pegmatites. Economic Geology, 78, 854–874.

Orville, P.M. (1963) Alkali ion exchange between vapor and feldspar phases. American Journal of Science, 261, 201–237.

Ovchinnikov, L.N. (1976) Lithochemical methods of prospecting rare metal pegmatites. Academy of Sciences USSR, 79 p. (in Russian; not seen) [transl. by the Department of the Secretary of State, Ottawa, Canada, 100 p.].

Ovchinnikov, L.N., and Solodov, N.A. (1971) Genetic types of cesium deposits and some problems of their exploration. Sovietskaya Geologiya, 7, 15–30 (in Russian; not seen) [transl. in Geochemistry International (1973), 14, 707–719].

Papike, J.J., Sherer, C.K., Simon, S.B., and Laul, J.C. (1983) Fluid flow through crystalline rocks: Sheet silicates as trace element traps (abs.). Geological Society of America Abstracts with Programs, 15, 658.

Pichavant, Michel. (1981) An experimental study of the effect of boron on water saturated haplogranite at 1 kbar vapour pressure. Contributions to Mineralogy and Petrology, 76, 430–439.

Rinaldi, R., Černý, Petr, and Ferguson, R.B. (1972) The Tanco pegmatite at Bernic Lake, Manitoba. VI. Lithium-rubidium-cesium micas. Canadian Mineralogist, 11, 690–707.

Shearer, C.K., Papike, J.J., Simon, S.B., Laul, J.C., and Christian, R.P. (1984) Pegmatite/wallrock interactions, Black Hills, South Dakota: Progressive boron metasomatism adjacent to the Tip Top pegmatite. Geochimica et Cosmochimica Acta, 48, 2563–2579.

Shearer, C.K., Papike, J.J., Simon, S.B., and Laul, J.C. (1986) Pegmatite/wallrock interactions, Black Hills, South Dakota: Interactions between pegmatite-derived fluids and quartz-mica schist wallrock. American Mineralogist, 71, 518–539.

Spear, F.S. (1977) An experimental study of hornblende stability and compositional variability in amphibolite. American Journal of Science, 281, 697–734.

Thomas, A.V., and Spooner, E.T.C. (1984) Petrological evidence for inward and upward non-replacive crystallization in the growth sequence of the lower wall zone, Ta (-Sn) bearing banded albitite beryl fringe to core, Tanco pegmatite, Manitoba (abs.). Geological Association of Canada–Mineralogical Association of Canada Program with Abstracts, 9, 111.

——— (1985) Occurrence, petrology, and fluid inclusions characteristics of tantalum mineralization in the Tanco pegmatite, southeastern Manitoba. In R.P. Taylor and D.F. Strong, Eds., Granite-related mineral deposits: Geology, petrogenesis, and tectonic settings, 274–278. Canadian Institute of Mining, Geology Division.

——— (1987) Fluid inclusions in the system H_2O-CH_4-NaCl from the border unit Tanco pegmatite, S.E. Manitoba (abs.). Geological Association of Canada–Mineralogical Association of Canada Program with Abstracts, 12, 95.

Trueman, D.L. (1978) Exploration methods in the Tanco mine area of southeastern Manitoba, Canada. Energy, 3, 293–297.

Trueman, D.L., and Černý, Petr. (1982) Exploration for rare-element granitic pegmatites. Mineralogical Association of Canada Short Course Handbook 8, 463–493.

Velde, Bruce. (1985) Clay minerals: A physico-chemical explanation of their occurrence. Elsevier, Amsterdam.

Wright, C.M. (1963) Geology and origin of the pollucite-bearing Montgary pegmatite, Manitoba. Geological Society of America Bulletin, 74, 919–946.

Manuscript received January 8, 1987
Manuscript accepted July 9, 1987